Coupling between Current and Dynamic Magnetization
from Domain Walls to Spin Waves

Lucassen, Mathies Emile

Coupling between Current and Dynamic Magnetization
from Domain Walls to Spin Waves
Instituut voor Theoretische Fysica
Universiteit Utrecht
ISBN: 978-90-393-5793-4
Cover design: Joaquin Jonkman
Printed by Ipskamp Drukkers BV

Coupling between Current and Dynamic Magnetization
from Domain Walls to Spin Waves

Koppeling tussen stroom en dynamische magnetisatie
van domeinwanden tot spingolven
(met een samenvatting in het Nederlands)

Proefschrift

ter verkrijging van de graad van doctor aan de Universiteit Utrecht op gezag van de rector magnificus, prof. dr. G.J. van der Zwaan, ingevolge het besluit van het college voor promoties in het openbaar te verdedigen op woensdag 16 mei 2012 des middags te 2.30 uur

door

Mathies Emile Lucassen

geboren op 10 februari 1981 te Gouda

Promotor: Prof.dr.ir. H.T.C. Stoof
Co-promotor: Dr. R.A. Duine

This thesis is based on the following publications:

- M.E. Lucassen and R.A. Duine, 'Fluctuations of current-driven domain walls in the nonadiabatic regime', Physical Review B **80**, 144421 (2009).
- M.E. Lucassen and R.A. Duine, 'Spin motive forces and current fluctuations due to Brownian motion of domain walls', Solid State Communications **150**, 538-542 (2010).
- M.E. Lucassen, G.C.F. Kruis, R. Lavrijsen, H.J.M. Swagten, B. Koopmans, and R.A. Duine, 'Spin motive forces due to magnetic vortices and domain walls', Physical Review B **84**, 014414 (2011).
- M.E. Lucassen, C.H. Wong, R.A. Duine, and Y. Tserkovnyak, 'Spin-transfer mechanism for magnon-drag thermopower', Applied Physics Letters **99**, 262506 (2011).

Other publications:

- M.E. Lucassen, H.J. van Driel, C. Morais Smith, and R.A. Duine, 'Current-driven and field-driven domain walls at nonzero temperature', Physical Review B **79**, 224411 (2009).
- D. Culcer, M.E. Lucassen, R.A. Duine, and R. Winkler 'Current-induced spin torques in III-V ferromagnetic semiconductors', Physical Review B **79**, 155208 (2009).

Contents

Chapter 1

Introduction

In ferromagnetic materials below the Curie temperature, the local magnetization aligns in magnetic domains [1]. The place where two domains with different magnetization meet is called a domain wall. One can engineer samples such that one has two well-defined domains with opposite magnetization, with a well-defined domain wall. This is illustrated in Fig. 1.1. With a magnetic field or an electric current, the size of one

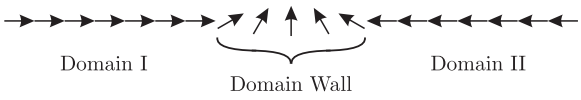

Figure 1.1: Cartoon of a ferromagnetic material with two magnetic domains. The border between the domains is called a domain wall.

domain can be increased at the cost of the other, thus moving the domain wall.

Current-driven domain-wall motion is part of a relatively new field of research, called 'spintronics'. In spintronics, not only the electron charge is used to operate a device, like in electronics, but also the spin of the electrons. One of the most well-known examples in this field is giant magnetoresistance [2, 3] and the related tunneling magnetoresistance. Giant magnetoresistance uses a setup with two layers: one fixed ferromagnet and one ferromagnet of which the magnetization can be parallel or antiparallel to that of the fixed layer. A current that is passed through these layers polarizes in the first layer. When the current enters the second layer, it experiences a different resistance for an antiparallel configuration than for a parallel configuration. In this way, the magnetization of the free ferromagnet can be read out by measuring the resistance. A setup for tunneling magneto resistance is similar, but has an additional insulating layer between the ferromagnetic layers. Modern readheads of hard drives

in computers are based upon this. Many more ideas have emerged, such as a magnetic racetrack memory [4], where a line of small magnetic domains can be shifted in order to read or write one of the domains without moving the read or write head. This idea uses current-driven domain-wall motion [5–8].

One of the central questions in spintronics is how current couples to magnetization, and more particularly to domain walls. For applications, it is important to have domain-wall motion for the lowest possible electric current, not only to reduce energy consumption, but also to reduce Joule heating. Reduction of the necessary current is closely related to the so-called "β parameter", which is much debated in the field. This parameter describes (in part) the strength of the coupling between current and domain walls. The domain-wall dynamics due to electron currents, and particularly the role of the β parameter, is the central subject of this thesis.

1.1 Landau-Lifschitz-Gilbert equation

Describing the exact motion of conduction electrons (the current), the atomic nuclei, and the localized electrons that orbit the atomic nuclei, while taking into account all their interactions, is an impossible task. We therefore consider a simplified model where the localized electrons and atomic nuclei are described by a continuous magnetization density $\mathbf{M}(\mathbf{x},t) = M_s\hat{\mathbf{\Omega}}(\mathbf{x},t)$, with M_s the saturation magnetization density and $\hat{\mathbf{\Omega}}(\mathbf{x},t)$ a unit vector at position $\mathbf{x}$ and time t. We assume that the magnetization has a constant magnitude M_s, which implies that the temperature is well below the Curie temperature. For notational convenience, we drop the argument of $\hat{\mathbf{\Omega}}$ from here onward.

The equation of motion for the magnetization direction in a ferromagnet is given by the Landau-Lifschitz-Gilbert equation [1]

$$\frac{\partial\hat{\mathbf{\Omega}}}{\partial t} = \gamma\hat{\mathbf{\Omega}}\times(\mathbf{H}_{\text{eff}}+\boldsymbol{\eta}) - \alpha\hat{\mathbf{\Omega}}\times\frac{\partial\hat{\mathbf{\Omega}}}{\partial t}\,, \tag{1.1}$$

where $\gamma = M_s/S$ is the gyromagnetic ratio (S is the spin density, we choose M_s and S to be positive), $\mathbf{H}_{\text{eff}}$ is the effective magnetic field and α is the Gilbert damping parameter. The stochastic field $\boldsymbol{\eta}$ describes thermal fluctuations and is discussed in more detail in Chapters 2 and 3. The first term on the right-hand side of Eq. (1.1) describes precessional motion of the local magnetization around the (effective) magnetic field. Note that this term preserves energy $\propto \mathbf{H}_{\text{eff}}\cdot\mathbf{\Omega}$. The damping α in the second term of Eq. (1.1) pulls the magnetization perpendicularly to the rotational motion towards the magnetic field direction. This term is a dissipative term since it decreases the energy of the system. The two terms in Eq. (1.1) are illustrated in Fig. 1.2. The effective field

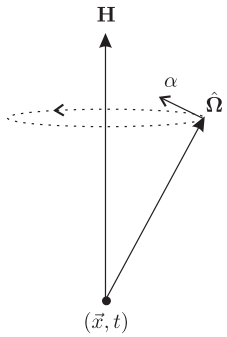

Figure 1.2: Precession (dotted line) of the local magnetization $\mathbf{\Omega}(\vec{x},t)$ around the (effective) magnetic field $\mathbf{H}$. The arrow pointing perpendicular to the circular motion denotes the direction of the damping proportional to α.

can be written as a micromagnetic contribution $\mathbf{H}_0$ and a contribution from current. The contribution $\gamma\mathbf{H}_0 = -\frac{1}{\hbar}\partial_{\mathbf{\Omega}}\mathcal{F}$ is the effective field that determines the equilibrium magnetization direction. It is the functional derivative of the micromagnetic energy functional $\mathcal{F}$ that includes anisotropies K_i in the i-direction, external magnetic field $\mathbf{B}_{\text{ext}}$ and external potentials V_{ext}, and is to lowest order in $\mathbf{\Omega}$ given by

$$\mathcal{F} = \int \frac{d\vec{x}}{a^3}\left(-J\mathbf{\Omega}\cdot\nabla^2\mathbf{\Omega} + K_i\hat{\Omega}_i^2 - g\mathbf{B}_{\text{ext}}\cdot\mathbf{\Omega} + V_{\text{ext}}\right) . \tag{1.2}$$

Here, J is the exchange coupling, a is the lattice spacing, and g is the g-factor. A sum over index $i \in \{x,y,z\}$ is implied. In this functional, we neglect dipole-dipole interactions. Besides these equilibrium contributions we consider conduction-electron currents in the material that affect the magnetization. For smoothly varying magnetization, an important contribution of the current to the equations of motion for the magnetization is spin-transfer torque.

1.2 Spin-transfer torque

Although current-driven domain wall motion was already predicted [5] and experimentally observed [6] in the 1980's, the idea of spin-transfer torque was first put forward as recently as 1996 [7, 8]. The idea is as follows: when an electric current density $\vec{j}$ is driven through a ferromagnet, it is polarized, *i.e.*, the expectation value of the spins of the conduction electrons is pointing in the direction of the magnetization of the ferromagnet. Therefore, there is a net spin current density $\vec{j}_{\text{s}} = -\hbar\mathcal{P}\vec{j}/|e|$,

where $\mathcal{P} = (\sigma_\uparrow - \sigma_\downarrow)/\sigma$ is the current polarization, $\sigma_\uparrow$ and $\sigma_\downarrow$ are majority and minority electron conductivities, respectively, and $\sigma = \sigma_\uparrow + \sigma_\downarrow$ is the total conductivity. When a current is passed through a sample with two domains with opposite magnetization, the current polarizes in the direction of the first domain it encounters. The current then flows into the second domain and adjusts itself to the local magnetization there (we assume that the electrons follow the local magnetization adiabatically, which is true for smoothly varying magnetization). The situation is sketched in Fig. 1.3. If

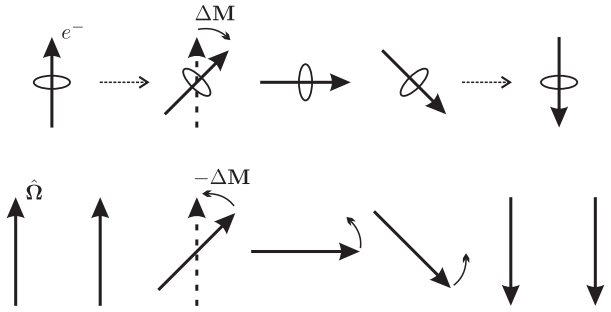

Figure 1.3: Cartoon of adiabatic spin-transfer torque of conduction electrons on a domain wall. The top arrows denote the spin of the electrons that move from left to right. As the electrons follow the magnetization direction $\mathbf{\Omega}$ (bottom arrows) adiabatically, the electron spin changes. This angular momentum $\Delta\mathbf{M}$ is transferred to the local magnetization, which leads to domain-wall motion to the right.

angular momentum is conserved, the change in magnetization of the conduction electrons is transferred to the local magnetization. In other words, the polarized current has exerted a torque on the magnetization of the ferromagnet. The effect in the case of two domains is that the first domain grows and that the second domain shrinks, *i.e.*, the border between the domains (the domain wall) moves. The change in local magnetization due to the torque described above is given by

$$\frac{\partial \mathbf{\Omega}}{\partial t}|_{\text{ad}} = -\frac{\hbar \mathcal{P}}{2S|e|}\,(j_i \nabla_i)\,\mathbf{\Omega}\,, \tag{1.3}$$

where summation over the index i is implied. This contribution is called the 'adiabatic' spin-transfer torque.

There are, however, numerous processes that make the electrons act differently than in the above situation [9, 10]. In general, there are two directions for the change of the electron spin density: in the direction of the local-magnetization gradient (as

described above) and perpendicular to it. Since the direction of the spin density of the electrons now has a component perpendicular to the local-magnetization gradient, this dissipative contribution to the spin-transfer torque acts perpendicular to the adiabatic spin-transfer torque

$$\frac{\partial \mathbf{\Omega}}{\partial t}|_{\mathrm{sf}} = -\beta \mathbf{\Omega} \times \left(\frac{\hbar \mathcal{P}}{2S|e|} j_i \nabla_i \right) \mathbf{\Omega} \,. \tag{1.4}$$

Here, β is a phenomenological parameter, and again summation over the index i is implied. Zhang and Li [9] compute a contribution to β from spin flips in a relaxation-time approximation $\beta = \tau_{\mathrm{ex}}/\tau_{\mathrm{sf}}$. Here, $\tau_{\mathrm{ex}} = \hbar S/J_{\mathrm{ex}}$ is a time scale associated with the exchange interaction between the local magnetization and conduction electrons and τ_{sf} is the spin-flip time. There are more effects that contribute to β, such as spin-orbit coupling and impurity scattering.

There is some discussion on what physical name the β parameter should have. It is sometimes referred to as 'non-adiabatic spin-transfer torque', simply because it is not the adiabatic spin-transfer torque as defined in Eq. (1.3). However, others argue that the label 'non-adiabatic' should be reserved for terms that are higher order in gradients, and propose the name 'dissipative spin-transfer torque' because of the dissipative nature of the contributions. In this thesis, we will use the latter name. We conclude that the change of the magnetization direction in the presence of current is given by the Landau-Lifschitz-Gilbert equation

$$\frac{\partial \mathbf{\Omega}}{\partial t} = \gamma \mathbf{\Omega} \times \mathbf{H}_0 - \alpha \mathbf{\Omega} \times \partial_t \mathbf{\Omega} - \frac{\hbar \mathcal{P}}{2S|e|} j_i \left(1 + \beta \mathbf{\Omega} \times\right) \nabla_i \mathbf{\Omega} \,. \tag{1.5}$$

1.3 Linear momentum transfer

In the previous section, we considered electric currents that flow through a domain wall without scattering off the domain wall. This description is valid for smoothly varying magnetization textures. For gradients on length scales smaller than the spin-diffusion length, linear momentum transfer starts to play a role [11]. When the electrons encounter a large change in magnetization, such as a sharp domain wall, the electrons get reflected and their momentum is altered. This change in momentum is transferred to the domain wall. In the special case of rigid domain walls, this contribution turns out to act in the same way as the dissipative spin-transfer torque. Therefore, in the case of a rigid domain wall, linear momentum transfer gives a contribution to an effective β parameter. Note that this contribution is truly non-adiabatic. We study linear momentum transfer in more detail in Chapter 2, where we compute explicitly the reflection and transmission coefficients for electrons that encounter a (sharp) domain wall .

1.4 Spin motive force

There is an inverse effect to the spin-transfer torque, where the magnetization is not affected by the moving conduction electron spins, but the other way round: the conduction electron spins experience a force due to a time-dependent magnetization texture. This effect is called the spin motive force [12–16]. In this section, we make this intuitive relation more specific and derive a general expression for the force that the electrons experience.

Since the relation between spin-transfer torque and spin motive force is based on Onsager reciprocity, we first need to choose suitable variables and their thermodynamical conjugates. We loosely follow Tserkovnyak and Mecklenburg in Ref. [14], and write the equations of motion in terms of particle density $\rho(\vec{x},t)$ rather than electric current $\vec{j}$ using the continuity equation $\partial_t \rho = -\nabla_i j_i/|e|$. The thermodynamical conjugate to ρ is the chemical potential $\mu = -\partial_\rho \mathcal{F}$ that takes the place of an electric potential. Note that the current in Eq. (1.5) is driven by a gradient in the chemical potential $j_i = \sigma \nabla_i \mu/|e|$. The other variable is the magnetization density $M_\mathrm{s}\mathbf{\Omega}$ whose thermodynamical conjugate is the (negative) effective field $\mathbf{H}_0 = -\frac{1}{\gamma\hbar}\partial_{\mathbf{\Omega}}\mathcal{F} = -\partial_{\boldsymbol{M}}\mathcal{F}$, as we stated above. We write the equations of motion as

$$\begin{pmatrix} \partial_t \rho \\ \\ M_\mathrm{s}\partial_t \Omega_\alpha(\vec{x},t) \end{pmatrix} = \begin{pmatrix} -\frac{\sigma}{e^2}\nabla^2 & \gamma_{1,2} \\ \\ \gamma_{2,1} & \varepsilon_{\alpha\beta\gamma}\Omega_\beta \end{pmatrix} \cdot \begin{pmatrix} \delta_{\alpha\gamma}\mu \\ \\ H_{0,\gamma} \end{pmatrix} , \tag{1.6}$$

where $\gamma_{2,1} = -(\gamma\hbar\mathcal{P}\sigma/2e^2)(\delta_{\eta\gamma} + \beta\varepsilon_{\beta\eta\gamma}\Omega_\beta)\nabla_i\Omega_\eta\nabla_i$ using the spin-transfer torque equation (1.5). Here, summation over the spin-space indices β,γ and η is implied and $\varepsilon_{\alpha\beta\gamma}$ is the Levi-Civita pseudotensor. From Onsager reciprocity we know that $\gamma_{1,2} = -\gamma_{2,1}$ (the (-) sign comes from the fact that the effective field is odd under time reversal), such that the change in electron density due to an effective field is (note that we set $\mu = 0$, *i.e*, the change in density is only driven by magnetization dynamics, and not by an external electric field)

$$\partial_t \rho = \frac{\gamma\hbar\mathcal{P}\sigma}{2e^2}(\nabla_i \mathbf{H}_0)\cdot(1+\beta\mathbf{\Omega}\times)\nabla_i\mathbf{\Omega}\,. \tag{1.7}$$

Up to first order in $\nabla\mathbf{\Omega}$, *i.e.*, for slowly varying magnetization, we can write the gradient of the effective field as a total gradient and use the continuity equation $\partial_t\rho = -\nabla_i j_i/|e|$ to identify the current density induced by magnetization dynamics

$$j_i = -\frac{\gamma\hbar\mathcal{P}\sigma}{2|e|}\mathbf{H}_0\cdot(1+\beta\mathbf{\Omega}\times)\nabla_i\mathbf{\Omega}\,. \tag{1.8}$$

The effective field itself can be expressed in terms of the magnetization dynamics using the spin-transfer torque equation (1.5)

$$\mathbf{H}_0 = -\frac{1}{\gamma}(\mathbf{\Omega} \times \partial_t \mathbf{\Omega}) \,. \tag{1.9}$$

Here, we ignored the term due to currents, since this is generated by the magnetization dynamics itself. This backreaction therefore only gives rise to higher order terms in $\nabla\mathbf{\Omega}$. We substitute Eq. (1.9) into Eq. (1.8) to find an expression for the induced current density due to magnetization dynamics up to first order in gradient terms [12, 15]

$$j_i = \frac{\hbar \mathcal{P}\sigma}{2|e|}\left[\mathbf{\Omega}\cdot(\partial_t\mathbf{\Omega}\times\nabla_i\mathbf{\Omega}) + \beta(\partial_t\mathbf{\Omega}\cdot\nabla_i\mathbf{\Omega})\right] \,. \tag{1.10}$$

Note that this expression gives the current density at position $\vec{x}$ and time t. The current density that is observed at the ends of the sample is obtained by averaging this quantity over the sample. As a last remark, we note that the current can also be written as a force on the electrons. We define forces that drive majority and minority particle currents $\vec{j}_\alpha = \sigma_\alpha \vec{F}_\alpha / e^2$, with $\alpha \in \{\uparrow,\downarrow\}$. Combining $\vec{j}_\mathrm{s} = \hbar\mathcal{P}\vec{j}/|e|$ with $\vec{j}_\mathrm{s} = \hbar(\vec{j}_\uparrow - \vec{j}_\downarrow)$ and $\vec{j} = |e|(\vec{j}_\uparrow + \vec{j}_\downarrow)$, it is easy to see that $\vec{j}_\uparrow/\sigma_\uparrow = -\vec{j}_\downarrow/\sigma_\downarrow$. Therefore, $\vec{F}_\uparrow = -\vec{F}_\downarrow = \vec{F}$. We then write $\vec{j} = |e|(\vec{j}_\uparrow + \vec{j}_\downarrow) = (\sigma_\uparrow - \sigma_\downarrow)\vec{F}/|e|$ to identify the force on the conduction electrons (which is opposite for opposite spins)

$$F_i = \frac{\hbar}{2}\left[\mathbf{\Omega}\cdot(\partial_t\mathbf{\Omega}\times\nabla_i\mathbf{\Omega}) + \beta(\partial_t\mathbf{\Omega}\cdot\nabla_i\mathbf{\Omega})\right] \,. \tag{1.11}$$

Note that in deriving this result, we have ignored Gilbert damping. However, it turns out that this does not alter the result in Eqs. (1.10) and (1.11) [14].

1.5 Rigid domain walls

In this section, we apply the derivations so-far to rigid domain walls. In experiment, the exact form of a domain wall is determined by details of the sample, such as geometry and anisotropies. In many experiments this leads to a vortex domain wall, depicted in Fig. 1.4 (a).

The complexity of this configuration makes an analytic theoretical analysis difficult. We treat these walls numerically in Chapter 4. Another wall that might form is a transverse domain wall. This simpler configuration can be described by a domain wall line, illustrated in Fig. 1.4 (b). Here, the position of the domain wall is a function of the coordinate along the width of the sample. For realistic transverse domain walls, it turns out that the center of the domain wall lies on a diagonal line. If we simplify this

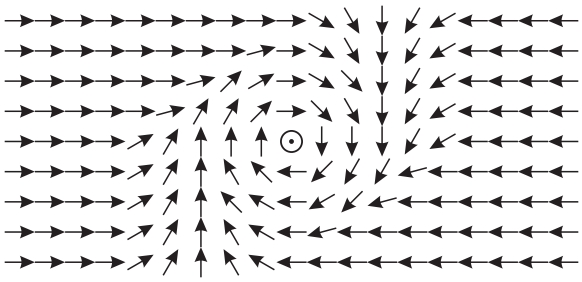

(a)

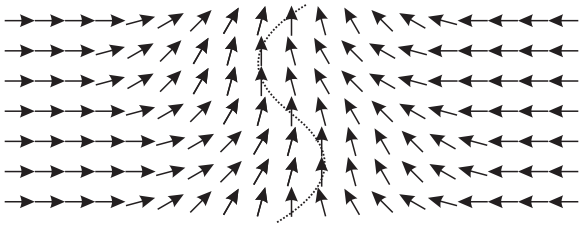

(b)

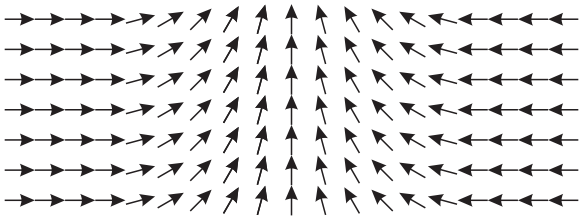

(c)

Figure 1.4: Graphical depiction of head-to-head domain wall configurations: a vortex domain wall (a), a domain-wall line (b), and a rigid domain wall (c).

even further with the demand that the domain wall position is not a function of the coordinate along the width of the sample, we arrive at a rigid domain wall, shown in Fig. 1.4 (c). In the cartoon for a rigid domain wall in Fig. 1.4 (c), we use Eq. (1.2) with $K_x = -K_{\text{easy}}$ (x is the horizontal axis) and $K_z = K_\perp$ (z is perpendicular to the paper), with K_{easy} and $K_\perp$ positive, we set $B_{\text{ext}} = 0$ and $V_{\text{ext}=0}$.

For this simplified domain wall we can make an ansatz which allows us to compute

several characteristics analytically. It turns out that many of these calculations work well not only for transverse domain walls, but also for vortex domain walls. The ansatz follows from the lowest energy configuration with head-to-head boundary conditions, *i.e.*, $\mathbf{\Omega}(x=-\infty) = -\mathbf{\Omega}(x=\infty) = \hat{x}$. We describe the magnetization at position $\vec{x}$ and time t as a unit vector with two angles $\theta(\vec{x},t)$ and $\phi(\vec{x},t)$ such that

$$\mathbf{\Omega}(\vec{x},t) = \begin{pmatrix} \cos[\theta(\vec{x},t)] \\ \sin[\theta(\vec{x},t)]\cos[\phi(\vec{x},t)] \\ \sin[\theta(\vec{x},t)]\sin[\phi(\vec{x},t)] \end{pmatrix} , \tag{1.12}$$

where we choose the x-direction along the easy-axis and the z-direction along the hard-axis (see Fig. 1.5). From the energy functional in Eq. (1.2) we derive that with

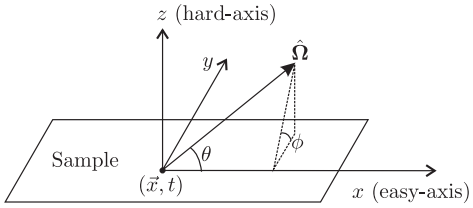

Figure 1.5: Definition of the axes x, y, z and angles θ, ϕ. In the case of most ferromagnetic strips, the hard-axis lies perpendicular to the sample and the easy-axis lies in the longitudinal direction. The choice of these axes does not alter the final results for a rigid domain wall.

head-to-head boundary conditions the lowest energy is obtained for

$$\theta(\vec{x},t) = 2\arctan\left\{e^{[x-X(t)]/\lambda}\right\} , \qquad \phi(\vec{x},t) = 0 , \tag{1.13}$$

with X the position of the domain wall. Note that the angles do not depend on y and z, since we describe a rigid domain wall. The width of the domain wall is determined by a competition between the exchange coupling J and the easy-axis anisotropy K_{easy} and is given by $\lambda = \sqrt{J/K_{\text{easy}}}$.

The conjugate momentum of the domain wall position $X(t)$ is the chirality $\phi(t)$. To obtain the dynamics, we therefore let the configuration deviate from the lowest energy by introducing a time-dependent chirality $\phi(\vec{x},t) = \phi(t)$. In this way, the domain wall is described by two coordinates: the position $X(t)$ and the chirality $\phi(t)$. We insert the

ansatz into Eq. (1.5) to obtain equations of motion for a rigid domain wall [11]

$$\begin{aligned}\dot{\phi}+\alpha\frac{\dot{X}}{\lambda}&=\gamma H_{\text{ext}}+\beta\frac{\hbar\mathcal{P}}{2\lambda S|e|}j+\frac{\lambda}{\hbar}\frac{\partial V_{\text{ext}}}{\partial X}+\eta_1\,,\\ \frac{\dot{X}}{\lambda}-\alpha\dot{\phi}&=\frac{K_\perp}{\hbar}\sin(2\phi)+\frac{\hbar\mathcal{P}}{2\lambda S|e|}j+\eta_2\,.\end{aligned}\tag{1.14}$$

Here, the current j is the x-component of the full current and the external field H_{ext} is chosen along the x-direction[1], $K_\perp$ is the hard-axis anisotropy, *i.e.*, the anisotropy perpendicular to the sample. We introduced two separate gaussian stochastic fields η_1 and η_2 that describe thermal fluctuations and are on average zero. Note that these fields are no longer vectors. The strength of the stochastic fields η_i is determined by the fluctuation-dissipation theorem[2]

$$\langle\eta_i(t)\eta_j(t')\rangle=\delta_{i,j}\delta(t-t')\frac{2\alpha k_{\text{B}}T}{\hbar N}\,.\tag{1.15}$$

1.5.1 Rigid-domain-wall motion

For $V_{\text{ext}}=0$, the problem of a rigid domain wall in Eqs. (1.14) is equivalent to that of an overdamped particle in a washboard potential. The washboard pattern is caused by the hard-axis anisotropy $K_\perp$. Due to currents and external fields, the washboard is tilted in two directions, see Fig. 1.6. Let us first consider only a magnetic field. The magnetic field tilts the energy landscape in the X-direction. At the same time, the Gilbert damping terms in Eqs. (1.14) drive the domain wall in a perpendicular direction up the side of the valley, where it will remain at a fixed value for ϕ. In this way, the position of the domain wall increases while the chirality is fixed. For a certain value of the external field, however, the damping terms are large enough to push the domain wall over the barrier, thus releasing the chirality. This leads to oscillatory motion in the position of the domain wall, which decreases the average velocity. This

[1] More generally, since the current couples to a gradient of the magnetization, there is only one component of the current that contributes, *i.e.*, the component along the change in magnetization. The magnetic field, however, couples to the magnetization itself and therefore contributes in all directions. For a rigid domain wall, the magnetic field should be chosen along the easy-axis (note that this is not necessarily the same direction as the current. For example, in perpendicularly magnetized materials, the easy-axis points out of the sample). It turns out to be hard to consider magnetic fields that are not chosen along the easy-axis due to their effect on the boundary conditions.

[2] From the Fokker-Planck equation, one can show rigorously that this is the right way of introducing thermal fluctuations, *i.e.*, in this way the Boltzmann equilibrium is a time-independent solution to the Fokker-Planck equation. The procedure is explained in more detail in Ref. [18]. In Chapter 2 we present an alternative way of deriving the appropriate terms in the equations of motion that include thermal fluctuations and their correlations by making use of the Keldysh formalism.

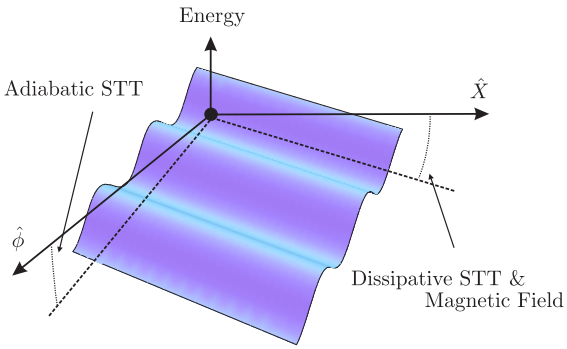

Figure 1.6: Potential landscape for a rigid domain wall (black dot). The adiabatic spin-transfer torque causes a gradient in the energy along the ϕ-direction, the dissipative spin-transfer torque and the magnetic field tilt the energy landscape in the X-direction.

phenomenon is known as Walker breakdown, the field at which it occurs is the Walker field $\gamma H_{\rm W} = \alpha K_\perp/\hbar$. From Eqs. (1.14), the velocity can be computed for $T = 0$

$$\langle \dot{X} \rangle = \frac{\lambda\gamma}{\alpha}\left[H_{\rm ext} - \frac{1}{1+\alpha^2}{\rm Re}\sqrt{H_{\rm ext}^2 - H_{\rm W}^2}\right], \tag{1.16}$$

where $\langle .. \rangle$ denotes a time average over one period of oscillation. The average velocity can also be computed for nonzero temperature, for more details we refer to Refs. [17, 18]. The curves are given in Fig. 1.7 (a). We see that temperature smoothes the cusps around Walker breakdown, which is understood from the fact that now the depinning of the chirality is thermally assisted.

For current-driven domain-wall motion without external magnetic field, the chirality is depinned in a more direct way since the adiabatic spin-transfer torque tilts the energy landscape in the ϕ-direction. The critical current for $\beta = 0$ is then given by $j_{\rm cr} = 2\lambda S|e|K_\perp/(\mathcal{P}\hbar^2)$. If we include β (which contributes to depinning via the Gilbert damping terms), the critical current is $j_{\rm cr} = 2\lambda S|e|K_\perp/(\mathcal{P}\hbar^2|1-\beta/\alpha|)$. Then, for $T = 0$, Eqs. (1.14) are solved by

$$\langle \dot{X} \rangle = \frac{\hbar\mathcal{P}}{2\alpha S|e|}\left[\beta j - \frac{\alpha-\beta}{1+\alpha^2}\,{\rm Re}\sqrt{j^2 - j_{\rm cr}^2}\right]. \tag{1.17}$$

Also in the results [17, 18] in Fig. 1.7 (b) for current-driven domain wall motion, we see a thermal smoothing around the depinning current. We note that the β parameter is of most importance for small applied currents $j < j_{\rm cr}$. For large currents $j \gg j_{\rm cr}$ Eq. (1.17) reduces to $\langle \dot{X} \rangle = -j\hbar\mathcal{P}/2S|e|$ (we ignore a factor $1+\alpha^2 \simeq 1$), independent

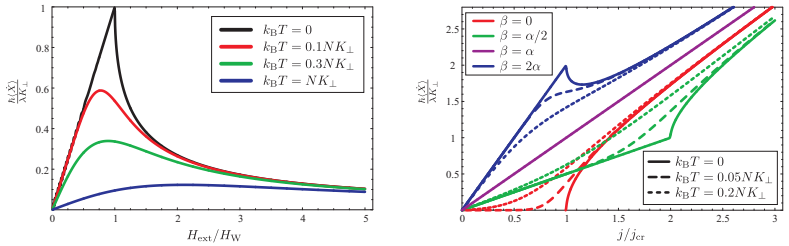

(a) (b)

Figure 1.7: Average domain-wall velocity as a function of an applied magnetic field (a) or current (b) for several temperatures and values of β.

of α and β. In this context, we should also spend some words on extrinsic pinning. In experiments, there will always be impurities. These random defects cause extrinsic pinning. Also, artificial deformations of a sample can cause domain wall pinning at a desired position. For the above description of a rigid domain wall, extrinsic pinning can be treated effectively as a potential well in the X-direction, *i.e.*, the external potential V_{ext} in Eqs. (1.14). For random impurities, a description in terms of a disorder potential is needed [18]. Note that random impurities are not always undesirable, and that they can be created on purpose via irradiation to affect sample properties [19]. In this thesis, we do not treat disorder pinning.

Both the results for current-driven and field-driven domain wall motion for a rigid domain wall turn out to capture the behavior of domain walls in experiment, at least qualitatively. In fact, also vortex domain-wall motion shows qualitatively similar behavior.

1.5.2 Spin motive forces due to rigid domain walls

Above, we have established the dynamics of a rigid domain wall that is driven by a magnetic field or a current. Now, we consider a situation where a domain wall is driven by an external magnetic field. Due to the dynamics of the domain wall, a current is induced via the spin motive force. To find the generated current density in terms of the collective coordinates X and ϕ, we insert the ansatz in Eq. (1.13) into Eq. (1.10) to find

$$j = \frac{\hbar \mathcal{P} \sigma}{|e| L} \left[\beta \frac{\dot{X}}{\lambda} - \dot{\phi} \right] , \tag{1.18}$$

where the current is in the same direction as the domain-wall velocity. We insert the solutions for field-driven domain-wall motion in Eq. (1.16) to arrive at the expression

$$\langle j \rangle = \frac{\gamma \hbar \mathcal{P} \sigma}{|e| L} \left[\frac{\beta}{\alpha} H_{\text{ext}} - \frac{1 + \beta/\alpha}{1 + \alpha^2} \text{Re} \sqrt{H_{\text{ext}}^2 - H_{\text{W}}^2} \right] , \tag{1.19}$$

where $\langle .. \rangle$ denotes a time-average. This is illustrated in Fig. 1.8. In Chapter 4, we look in more detail at spin motive forces, both for rigid domain walls and for vortex domain walls. It turns out that the expression for rigid domain walls does not capture the behavior seen in experiment [20]. We find that the behavior of the induced current for a vortex domain wall is qualitatively different than the expression for a rigid domain wall, and agrees with experiment.

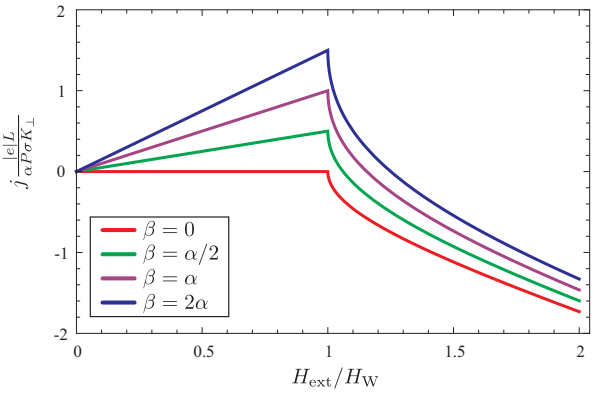

Figure 1.8: Induced current from spin motive force for a rigid domain wall as a function of the applied field for several values of β. Note that the current is averaged over time.

1.6 Outline

So-far, we have derived some general expressions for domain-wall motion and the spin motive force. We have seen that the β parameter plays a large role in both subjects. In all chapters of this thesis, there is an emphasis on the determination of this parameter.

We also know how to incorporate thermal fluctuations for rigid domain walls, as shown above. In Chapter 2, we study a different kind of fluctuations: shot noise. This noise is caused by the fact that an electric current consists of electrons, and therefore has fluctuations. In the process, we also compute transmission and reflection coefficients for a rigid domain wall, and from them the linear momentum transfer.

More work on fluctuations is done in Chapter 3. Here, we consider a (extrinsically pinned) rigid domain wall under the influence of thermal fluctuations that induces a current via spin motive force. We compute how the resulting noise in the current is related to the β parameter.

In Chapter 4 we look into in more detail into the spin motive forces from field-driven domain walls. Using micromagnetic simulations, we compute the spin motive force due to vortex domain walls explicitly. As mentioned before, this gives qualitatively different results than for a rigid domain wall.

The final subject in Chapter 5 is the application of the general expression for spin motive forces to magnons. Although this might seem to be unrelated to domain-wall motion, this calculation allows us to relate the β parameter to macroscopic transport coefficients.

This work was supported by Stichting voor Fundamenteel Onderzoek der Materie (FOM), the Netherlands Organization for Scientific Research (NWO), and by the European Research Council (ERC) under the Seventh Framework Program (FP7).

Chapter 2

Current-induced fluctuations of domain walls

Abstract

We outline a general framework to determine the effect of non-equilibrium fluctuations on driven collective coordinates, and apply it to a current-driven domain wall in a nanocontact. In this case the collective coordinates are the domain-wall position and its chirality, that give rise to momentum transfer and spin transfer, respectively. We determine the current-induced fluctuations corresponding to these processes and show that at small frequencies they can be incorporated by two separate effective temperatures. As an application, the average time to depin the domain wall is calculated and found to be lowered by current-induced fluctuations. It is shown that current-induced fluctuations play an important role for narrow domain walls, especially at low temperatures.

2.1 Introduction

Fluctuations play an important role in many areas of physics. The classic example is Brownian motion [21], for example of a colloidal particle in a suspension. The effect of collisions of the small particles, that constitute the suspension, with the colloid is modelled by stochastic forces. The strength of these forces is inferred from the famous fluctuation-dissipation theorem, which states that their variance is proportional to damping due to viscosity, and to temperature, and that their average is zero. If the suspension is driven out of equilibrium, the average force on the colloid will no longer be zero. Because of the non-equilibrium situation, the fluctuation-dissipation theorem in principle no longer holds, and the fluctuations cannot be determined from it anymore. Another explicit example of fluctuations in a driven system that do not obey the fluctuation-dissipation theorem is shot noise in the current in mesoscopic

conductors, where the fluctuations are determined by the applied voltage instead of temperature. It is ultimately caused by the fact that the electric current is carried by discrete charge quanta, the electrons [22].

The non-equilibrium system on which we focus in this chapter is a current-driven domain wall [5, 6] in a ferromagnetic conductor. Here the domain wall and the electrons play the role of the colloid and the suspension from the above example. As we have seen in Sections 1.2 and 1.3, there are two distinct processes that lead to current-induced domain-wall motion: spin transfer [7, 8] and momentum transfer [11]. Physically, momentum transfer corresponds to the force exerted on the domain wall by electrons that are reflected by the domain wall or transmitted with different momentum. Spin transfer corresponds to electrons whose spin follows the magnetization of the domain wall adiabatically, thereby exerting a torque on the domain wall. Most experiments [23–27] are in the adiabatic regime, where the electron spin follows the direction of magnetization adiabatically and where the spin-transfer torque is the dominant effect. The effect of spin relaxation on spin transfer in the adiabatic limit, leading to a dissipative spin-transfer torque, was discussed theoretically [9] and experimentally [28, 29]. The experiments by Feigenson *et al.* [30] with $SrRuO_3$ films, on the other hand, are believed to be in the non-adiabatic limit where domain walls are narrow compared to the Fermi wave length and momentum transfer is dominant. In this chapter, we will mostly consider narrow domain walls in nanocontacts [31–33].

Apart from the forces and torques on the magnetization texture due to nonzero average current, there are also current-induced fluctuations on the magnetization [34, 35] that ultimately have their origin in shot noise in the spin and charge current. Foros *et al.* [34] studied the effects of spin-current shot noise in single-domain ferromagnets, and found that for large voltage and low temperature the fluctuations are determined by the voltage and not by the temperature. Chudnovskiy *et al.* [36] study spin-torque shot noise in magnetic tunnel junctions, and in Ref. [37] Foros *et al.* consider a general magnetization texture and work out the current-induced magnetization noise and inhomogeneous damping in the adiabatic limit.

In this chapter, we determine the effect of current-induced fluctuations on a domain wall in the non-adiabatic limit. We show that it leads to anisotropic damping and fluctuations and show that the fluctuations can be described by two separate voltage-dependent effective temperatures corresponding to momentum transfer and spin transfer. We show that these effective temperatures differ considerably from the actual temperature for parameter values used in experiments with nanocontacts. From our model, we also determine the momentum transfer and the adiabatic spin-transfer torque on the driven domain wall, as well as the damping corresponding to these processes.

2.2 Model

In this section, we present a model for treating a domain wall out of equilibrium. We first develop a variational principle within the Keldysh formalism, and then work out the various Green's functions within Landauer-Büttiker transport.

2.2.1 Keldysh theory

We consider a one-dimensional model of spins coupled to conduction electrons. The action is on the Keldysh contour C given by

$$\begin{aligned} S[\mathbf{\Omega},\psi,\psi^*] = \int_C dt \Bigg\{ & -E_{\rm MM}[\mathbf{\Omega}] \\ & + \int \frac{dx}{a} \Bigg[-\hbar \mathbf{A}(\mathbf{\Omega}(x,t)) \cdot \frac{\partial \mathbf{\Omega}(x,t)}{\partial t} \\ & + \frac{\Delta}{2} \sum_{\sigma,\sigma'} \psi^*_\sigma(x,t) \mathbf{\Omega}(x,t) \cdot \boldsymbol{\tau}_{\sigma,\sigma'} \psi_{\sigma'}(x,t) \\ & + \sum_\sigma \psi^*_\sigma(x,t) \left(i\hbar \frac{\partial}{\partial t} + \frac{\hbar^2 \nabla^2}{2m} - V(x) \right) \psi_\sigma(x,t) \Bigg] \Bigg\} , \end{aligned} \tag{2.1}$$

where a is the lattice spacing, $\mathbf{A}(\mathbf{\Omega})$ is the fictitious vector potential that obeys $\boldsymbol{\nabla}_{\mathbf{\Omega}} \times \mathbf{A}(\mathbf{\Omega}) = \mathbf{\Omega}$ and ensures precessional motion of $\mathbf{\Omega}$, Δ is the exchange-splitting energy, $\mathbf{\Omega}(x,t)$ a unit vector in the direction of the magnetization, $\boldsymbol{\tau}$ the vector of Pauli matrices, and $V(x)$ an arbitrary scalar potential (Note that this is not the external potential $V_{\rm ext}$ in the energy functional for the magnetization in Eq. (1.2)). The fields $\psi^*_\sigma, \psi_\sigma$ represent the conduction electrons with spin projection $\sigma \in \{\uparrow,\downarrow\}$. The micromagnetic energy functional $E_{\rm MM}[\mathbf{\Omega}]$ is given by (this is the one-dimensional version of Eq. (1.2) with $B = 0$ and $V_{\rm ext} = 0$)

$$E_{\rm MM}[\mathbf{\Omega}] = -\int \frac{dx}{a} \left[J \mathbf{\Omega}(x,t) \cdot \vec{\nabla}^2 \mathbf{\Omega}(x,t) - K_\perp \Omega_y^2(x,t) + K_z \Omega_z^2(x,t) \right] , \tag{2.2}$$

with $J > 0$ the spin stiffness and $K_\perp > 0$ and $K_z > 0$ the hard- and easy-axis anisotropy constants, respectively. As we have seen in Section 1.5, the micromagnetic energy functional in Eq. (2.2) has stationary domain-wall solutions [11]

$$\mathbf{\Omega}(x) = (\sin\theta\cos\phi, \sin\theta\sin\phi, \cos\theta) . \tag{2.3}$$

These stationary solutions are the basis for a time-dependent variational ansatz which is given in one dimension by

$$\theta(\vec{x},t) = 2\arctan\left\{ e^{[x-X(t)]/\lambda} \right\} ; \qquad \phi(\vec{x},t) = \phi(t) , \tag{2.4}$$

where λ is the domain-wall width. In the above, we have taken the domain-wall position $X(t)$ to be time dependent. Furthermore, $\phi(t)$ is the angle of the magnetization at the center with the easy-plane, the so-called chirality. Using the above ansatz, the first two terms in the action in Eq. (2.1) simplify to

$$S_0[X,\phi] = \hbar N \int_C dt \left[\frac{\dot{X}}{\lambda}\phi - \frac{K_\perp}{2}\sin 2\phi \right] . \tag{2.5}$$

Here, $N = 2\lambda/a$ is the number of spins in the domain wall. Note that in three dimensions, the number of spins increases by a factor A/a^2, where A is the cross-sectional area of the sample.

Stochastic forces are not obtained in a natural way by variation of the real-time action or the Euclidean action of the system. The functional Keldysh formalism [38], however, provides us with the (current-induced and thermal) noise terms automatically, and is therefore more elegant for our purposes. By doing perturbation theory in the collective coordinates X and ϕ

$$\mathbf{\Omega} = \mathbf{\Omega}\Big|_0 + X\frac{\partial \mathbf{\Omega}}{\partial X}\Big|_0 + \phi\frac{\partial \mathbf{\Omega}}{\partial \phi}\Big|_0 + \text{h.o.} , \tag{2.6}$$

where from here onward the subscript $|_0$ denotes evaluation at $X = \phi = 0$, we derive an effective action on the Keldysh contour for the collective coordinates. We consider the low-frequency limit, which is a good approximation because the motion of the collective coordinates is on a much slower time scale than the electronic system.

The total action is now given by $S[X,\phi,\psi^*,\psi] = S_0[X,\phi] + S_C[X,\phi,\psi^*,\psi] + S_E[\psi^*,\psi]$. The contribution to the action in Eq. (2.1) that describes coupling between magnetization and electrons is up to first order given by

$$\begin{aligned} S_C[X,\phi]\Big|_0 = \frac{\Delta}{2}\int_C dt \int dx \sum_{\sigma,\sigma'} \psi^*_\sigma(x,t) \\ \left[(\partial_X \mathbf{\Omega}\cdot\boldsymbol{\tau})\Big|_0 X(t) + (\partial_\phi \mathbf{\Omega}\cdot\boldsymbol{\tau})\Big|_0 \phi(t) \right] \psi_{\sigma'}(x,t), \end{aligned} \tag{2.7}$$

where σ and σ' denote the spin of the electrons. The electron action reads

$$\begin{aligned} S_E[\psi^*,\psi] = \int_C dt \int dx \sum_{\sigma,\sigma'} \psi^*_\sigma(x,t) \\ \left[\left(i\hbar\frac{\partial}{\partial t} + \frac{\hbar^2\nabla^2}{2m} - V(x) \right)\delta_{\sigma\sigma'} - V_{\sigma\sigma'}(x) \right] \psi_{\sigma'}(x,t) , \end{aligned} \tag{2.8}$$

with the potential $V_{\sigma\sigma'}$, which arises from the zeroth order term $\mathbf{\Omega}|_0$, given in Eq. (2.21) below. The perturbation theory in X and ϕ enables us to derive an effective action on

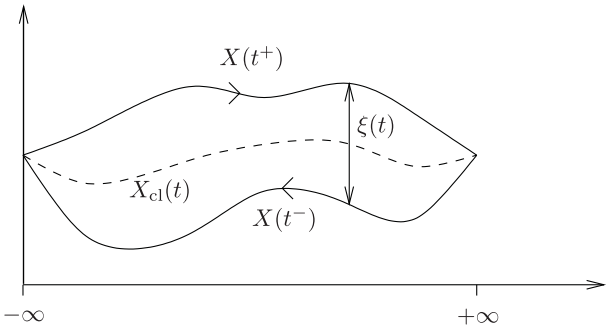

Figure 2.1: A path that the coordinate X might take on the Keldysh contour. The deviation from the (classical) mean path is denoted by $\xi(t)$.

the Keldysh contour for these coordinates

$$S_{\rm eff}[X,\phi] \simeq S_0[X,\phi] + \langle S_{\rm C}[X,\phi,\psi^*,\psi]\rangle + \frac{i}{2\hbar}\Big(\langle S_{\rm C}^2[X,\phi,\psi^*,\psi]\rangle - \langle S_{\rm C}[X,\phi,\psi^*,\psi]\rangle^2\Big) . \tag{2.9}$$

Here, the expectation values are taken with respect to the electron action $S_{\rm E}[\psi^*,\psi]$ in Eq. (2.8), *i.e.*,

$$\langle O[X,\phi,\psi^*,\psi]\rangle = \int d[\psi^*]d[\psi]e^{iS_{\rm E}[\psi^*,\psi]/\hbar}O[X,\phi,\psi^*,\psi] . \tag{2.10}$$

In the next section, we evaluate these expectation values in more detail.

Since we now have an effective action as a function of the collective coordinates X and ϕ, we can make use of the advantages of the Keldysh formalism. The effective action in Eq. (2.9) is integrated from $t=-\infty$ to $t=\infty$ and back. The forward and backward paths are different, as is shown for the coordinate X in Fig. 2.1, such that we write

$$X(t^\pm) = X_{\rm cl}(t) \pm \frac{\xi(t)}{2} ; \qquad \phi(t^\pm) = \phi_{\rm cl}(t) \pm \frac{\kappa(t)}{2} ;$$
$$\int_C dt\, f(t) = \int_{-\infty}^{\infty} dt^+ f(t^+) + \int_{\infty}^{-\infty} dt^- f(t^-) , \tag{2.11}$$

with the assumption that the variations ξ and κ are small. Furthermore, they obey the boundary conditions $\xi(\pm\infty) = \kappa(\pm\infty) = 0$. Integrating the effective action over

this contour and using the method outlined in Refs. [35, 38], we ultimately obtain the Langevin equations for a domain wall

$$\frac{\dot{X}_{\rm cl}(t)}{\lambda} - \alpha_\phi \dot{\phi}_{\rm cl}(t) = K_\perp \cos 2\phi_{\rm cl}(t) + F_\phi + \eta_\phi(t) \,, \tag{2.12}$$

$$\dot{\phi}_{\rm cl}(t) + \alpha_X \frac{\dot{X}_{\rm cl}(t)}{\lambda} = -F_X + \eta_X(t) \,. \tag{2.13}$$

The stochastic contributions η_ϕ and η_X in this expression arise via a Hubbard-Stratonovich transformation of terms quadratic in ξ and κ.

The expectation value of the action $S_C[X,\phi,\psi^*,\psi]$ in the effective action in Eq. (2.9) provide us with the forces

$$F_i = \frac{\Delta}{\hbar N} \sum_{\nu,\sigma,\sigma'} G^<_{\nu,\sigma,\sigma'}(0) \langle \nu,\sigma|\partial_i \mathbf{\Omega}|_0 \cdot \boldsymbol{\tau}|\nu,\sigma'\rangle \,, \tag{2.14}$$

with the index $i \in \{X/\lambda, \phi\}$. Note that in this expression, F_ϕ corresponds to spin transfer and F_X to momentum transfer. As we will see later on, $\partial_\phi \mathbf{\Omega}|_0 \cdot \boldsymbol{\tau}$ is associated with the divergence of the spin current, and $\partial_X \mathbf{\Omega}|_0 \cdot \boldsymbol{\tau}$ is associated with the force of the domain wall on the conduction electrons. The latter is, in the absence of disorder, proportional to the resistance of the domain wall [11]. The lesser Green's function in this expression is defined by $G_{\nu,\sigma,\sigma'}(t,t') = \theta(t,t') G^>_{\nu,\sigma,\sigma'}(t-t') + \theta(t',t) G^<_{\nu,\sigma,\sigma'}(t-t')$, where the Heaviside step functions are defined on the Keldysh contour. Note that the lesser Green's function in Eq. (2.14) is evaluated at equal times $t = t'$. Furthermore, we have expanded the Keldysh Green's function according to $\hat{i} G_{\sigma,\sigma'}(x,t;x',t') \equiv \langle \psi_\sigma(x,t) \psi^*_{\sigma'}(x',t')\rangle = \hat{i} \sum_\nu G_{\nu,\sigma,\sigma'}(t,t') \chi_{\nu,\sigma}(x) \chi^*_{\nu,\sigma'}(x')$, where χ and χ^* are electron eigenstates in the presence of a static domain wall that are labeled by ν. In terms of these states, the matrix elements are defined as

$$\int dx \, \langle \nu,\sigma|\hat{O}|\nu',\sigma'\rangle = \int dx \chi_{\nu,\sigma}(x) \hat{O}_{\sigma,\sigma'}(x) \chi^*_{\nu',\sigma'}(x) \,. \tag{2.15}$$

The damping terms in Eqs. (2.12) and (2.13) follow from the second-order terms in the perturbation theory in X and ϕ and read $\alpha_i = \mp {\rm Im}[\tilde{\Pi}^{(\pm)}_i(\omega)]/(N\hbar\omega)$ for $\omega \to 0$, with $\tilde{\Pi}^{(\pm)}(\omega)$ the response function given below. Since the action in Eq. (2.1) is quadratic in the electron fields, we use Wick's theorem to write the response function in terms of electron Green's functions

$$\begin{aligned}
\tilde{\Pi}^{(\pm)}_i(\omega) = {} & \mp \frac{\Delta^2}{4\hbar} \sum_{\nu,\nu'} \sum_{\sigma,\sigma'} \sum_{\rho,\rho'} \\
& \times \Big[G^>_{\nu,\sigma,\rho'}(\omega) G^<_{\nu',\rho,\sigma'}(-\omega) - G^<_{\nu,\sigma,\rho'}(\omega) G^>_{\nu',\rho,\sigma'}(-\omega) \Big] \\
& \times \langle \nu,\sigma|\partial_i \mathbf{\Omega}|_0 \cdot \boldsymbol{\tau}|\nu',\sigma'\rangle \langle \nu',\rho|\partial_i \mathbf{\Omega}|_0 \cdot \boldsymbol{\tau}|\nu,\rho'\rangle \,.
\end{aligned} \tag{2.16}$$

The functions $G^{>}(\pm\omega)$ and $G^{<}(\pm\omega)$ denote Fourier transforms of $G^{>}(\pm(t-t'))$ and $G^{<}(\pm(t-t'))$, respectively.

Without needing to assume (approximate) equilibrium, the Keldysh formalism provides us with an expression for the strength of the fluctuations in both coordinates $\langle\eta_i(t)\eta_j(t')\rangle = \hat{\imath}\delta_{i,j}\Pi_i^{\mathrm{K}}(t-t')/(\hbar N^2) \simeq \hat{\imath}\delta_{i,j}\tilde{\Pi}_i^{\mathrm{K}}(\omega=0)\delta(t-t')/(\hbar N^2)$ and $\langle\eta_i(t)\rangle = 0$. The Keldysh component of the response function contains similar matrix elements as the damping terms and is given by

$$\begin{aligned}\tilde{\Pi}_i^{\mathrm{K}}(\omega) = \frac{\Delta^2}{2\hbar}&\sum_{\nu,\nu'}\sum_{\sigma,\sigma'}\sum_{\rho,\rho'}\\ &\times\left[G^{>}_{\nu,\sigma,\rho'}(\omega)G^{<}_{\nu',\rho,\sigma'}(-\omega)+G^{<}_{\nu,\sigma,\rho'}(\omega)G^{>}_{\nu',\rho,\sigma'}(-\omega)\right]\\ &\times\langle\nu,\sigma|\partial_i\boldsymbol{\Omega}|_0\cdot\boldsymbol{\tau}|\nu',\sigma'\rangle\langle\nu',\rho|\partial_i\boldsymbol{\Omega}|_0\cdot\boldsymbol{\tau}|\nu,\rho'\rangle\,. \end{aligned} \tag{2.17}$$

We now define two separate effective temperatures

$$k_{\mathrm{B}}T_{\mathrm{eff},i} \equiv \frac{\hat{\imath}\tilde{\Pi}_i^{\mathrm{K}}(\omega=0)}{2\alpha_i N^2}\,. \tag{2.18}$$

These effective temperatures are defined such that Eqs. (2.12) and (2.13) obey the fluctuation-dissipation theorem with the effective temperatures. In the absence of a bias voltage, the effective temperatures reduce to the actual temperature divided by the number of spins in the system. More general, the effective temperatures are proportional to $1/N$, which is understood because they describe fluctuations in collective coordinates made up of N degrees of freedom [17]. We note that our formalism applies to any set of collective coordinates, and is not necessarily restricted to the example of a domain wall. We also point out that going beyond the low-frequency limit and taking into account the full frequency dependence in Eq. (2.17) leads to colored noise. In this case, effective temperatures may no longer be unambiguously defined [39].

2.2.2 Landauer-Büttiker transport

We now evaluate Eqs. (2.14–2.17) using the Landauer-Büttiker formalism, *i.e.*, the scattering theory of electronic transport. In order for this formalism to apply, the phase-coherence length L_ϕ must be larger than the domain-wall width λ. To compute the terms in the Langevin equations (2.12) and (2.13) explicitly, we need to find the matrix elements $\langle\nu,\sigma|\partial_i\boldsymbol{\Omega}|_0\cdot\boldsymbol{\tau}|\nu',\sigma'\rangle$ and the Green's functions. The Keldysh

Green's function is in terms of scattering states $\chi_\sigma^{\zeta\kappa\varepsilon}(x)$ given by

$$\begin{aligned}
&\hat{i}G_{\sigma,\sigma'}(x,t;x',t') \\
&= \int_0^\infty \frac{d\varepsilon}{2\pi} \sum_{\zeta,\kappa} \frac{2m/\hbar^2}{k_{\zeta\kappa}} e^{-\frac{\hat{i}}{\hbar}\varepsilon(t-t')} \chi_{\sigma'}^{\zeta\kappa\varepsilon}(x)[\chi_\sigma^{\zeta\kappa\varepsilon}(x')]^* \\
&\times \{\theta(t,t')[1-N_{\mathrm{F}}(\varepsilon-\mu_\zeta)] - \theta(t',t)N_{\mathrm{F}}(\varepsilon-\mu_\zeta)\}\,,
\end{aligned} \tag{2.19}$$

with μ_ζ the chemical potential of the lead on side $\zeta \in \{\mathrm{L(eft)},\mathrm{R(ight)}\}$, $\kappa \in \{\uparrow,\downarrow\}$ the spin of the incoming particles and $N_{\mathrm{F}}(x)$ the Fermi distribution function. We choose $V(x)=0$ for convenience. The momenta $k_{\zeta\kappa}$ associated with an energy ε are given by $k_{\mathrm{L}\uparrow} = k_{\mathrm{R}\downarrow} = k_{\mathbf{F}}\sqrt{(\varepsilon+\Delta/2)/\varepsilon_{\mathrm{F}}}$ and $k_{\mathrm{R}\uparrow} = k_{\mathrm{L}\downarrow} = k_{\mathbf{F}}\sqrt{(\varepsilon-\Delta/2)/\varepsilon_{\mathrm{F}}}$, where $k_{\mathbf{F}} = \sqrt{2m\varepsilon_{\mathrm{F}}/\hbar^2}$, with ε_{F} the Fermi energy in the leads. Note that the index ν used earlier now contains information on the origin, spin and energy of the incoming particle. We define the asymptotic expression for the scattering states in terms of transmission and reflection coefficients,

$$\chi_\sigma^{\mathrm{L}\kappa\varepsilon} = \begin{cases} \delta_{\sigma,\kappa} e^{\hat{i}k_{\mathrm{L}\kappa}x} + \delta_{\sigma,\gamma}\sqrt{\frac{k_{\mathrm{L}\kappa}}{k_{\mathrm{L}\gamma}}} r_{\gamma\kappa}(\varepsilon) e^{-\hat{i}k_{\mathrm{L}\gamma}x}, & x\to-\infty\,; \\ \\ \delta_{\sigma,\gamma}\sqrt{\frac{k_{\mathrm{L}\kappa}}{k_{\mathrm{R}\gamma}}} t_{\gamma\kappa}(\varepsilon) e^{\hat{i}k_{\mathrm{R}\gamma}x}, & x\to+\infty\,, \end{cases} \tag{2.20}$$

where summation over the spin index $\gamma \in \{\uparrow,\downarrow\}$ is implied, and with a similar expression for right-incoming particles. One example of such a scattering process is illustrated in Fig. 2.2. From the explicit form of the ansatz, it is easily seen that $\partial\mathbf{\Omega}/\partial X = -\partial\mathbf{\Omega}/\partial x$ which enables us to write $(\Delta/2)(\partial\mathbf{\Omega}/\partial X)|_0 \cdot \boldsymbol{\tau}_{\sigma,\sigma'} = \partial_x V_{\sigma,\sigma'}(x)$. Here ∂_x denotes a derivative with respect to x, and the potential is given by

$$V_{\sigma\sigma'}(x) = -\frac{\Delta}{2} \begin{pmatrix} \cos\theta_{\mathrm{dw}} & \sin\theta_{\mathrm{dw}} \\ \\ \sin\theta_{\mathrm{dw}} & -\cos\theta_{\mathrm{dw}} \end{pmatrix}\Bigg|_0 . \tag{2.21}$$

Furthermore, one can check that $(\partial\mathbf{\Omega}/\partial\phi)\cdot\boldsymbol{\tau}_{\sigma\sigma'}|_0 = -(\boldsymbol{\tau}_{\sigma\sigma'}\times\mathbf{\Omega})|_0^z$, where uppercase z denotes the z component of this cross product. The expectation value of this quantity is directly related to the divergence of the spin-current J_{s}^z, which measures the z component of the total spin-current

$$\partial_x J_{\mathrm{s}}^z(x) = \frac{\Delta}{2}\sum_{\sigma,\sigma'} \chi_\sigma^*(x)\Big[\boldsymbol{\tau}_{\sigma\sigma'}\times\mathbf{\Omega}(x)\Big]_0^z \chi_{\sigma'}(x)\,. \tag{2.22}$$

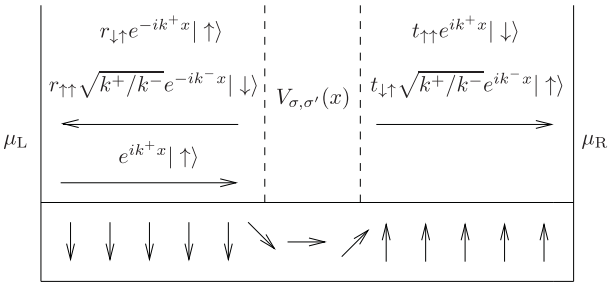

Figure 2.2: The asymptotic form of the scattering state for a particle coming in from the left with spin up, *i.e.* the state $\chi_\sigma^{\mathrm{L}\uparrow\varepsilon}$. We denoted $k^\pm = k_{\mathrm{F}}\sqrt{(\varepsilon \pm \Delta/2)/\varepsilon_{\mathrm{F}}}$, μ_{L} and μ_{R} are the chemical potentials in the left and right reservoir, respectively. The arrows on the bottom indicate the magnetization direction, the electrons experience a potential at the position of the domain wall.

In this expression, χ is a solution to the zeroth order time-independent Schrödinger equation with the potential $V_{\sigma,\sigma'}(x)$. The spin current is defined as

$$J_{\mathrm{s}}^z(x) = \frac{\hbar^2}{4mi}\sum_{\sigma,\sigma'}\Big\{\chi_\sigma^*(x)\tau^z_{\sigma\sigma'}[\partial_x\chi_{\sigma'}(x)] - [\partial_x\chi_\sigma^*(x)]\tau^z_{\sigma\sigma'}\chi_{\sigma'}(x)\Big\}\,. \tag{2.23}$$

From this, we observe that F_ϕ determined by Eq. (2.14) is indeed proportional to the divergence of spin current and hence corresponds to spin transfer.

We define $\mu_{\mathrm{L}} = \mu + |e|V$ and $\mu_{\mathrm{R}} = \mu \simeq \varepsilon_{\mathrm{F}}$. The expressions for the Green's function and the scattering states in Eqs. (2.19) and (2.20) now allow us to write Eqs. (2.14–2.18) in terms of transmission and reflection coefficients, the applied voltage V, and $k_{\mathrm{F}}\lambda$. For example, the momentum transfer in Eq. (2.14), with $i = X$, is up to first order in $|e|V/\varepsilon_{\mathrm{F}}$ given by

$$\begin{aligned} F_X \simeq{}& \frac{|e|V}{2\pi\hbar N}k_{\mathrm{F}}\lambda \\ &\left[\sqrt{\frac{\varepsilon+\Delta/2}{\varepsilon_{\mathrm{F}}}}\Big(1 + R_{\uparrow\uparrow} - T_{\downarrow\downarrow} + R_{\uparrow\downarrow} - T_{\downarrow\uparrow}\Big)\right. \\ &\left.+\sqrt{\frac{\varepsilon-\Delta/2}{\varepsilon_{\mathrm{F}}}}\Big(1 + R_{\downarrow\downarrow} - T_{\uparrow\uparrow} + R_{\downarrow\uparrow} - T_{\uparrow\downarrow}\Big)\right], \end{aligned} \tag{2.24}$$

Here, the reflection and transmission coefficients are defined as $R_{\sigma\sigma'} = R_{\sigma\sigma'}(\varepsilon = \varepsilon_{\mathrm{F}})$ with $R_{\sigma\sigma'}(\varepsilon) \equiv |r_{\sigma\sigma'}(\varepsilon)|^2$, and equivalently for the transmission coefficients. Note

that, although the coefficients are evaluated at the Fermi energy, they also depend on the ratio Δ/ε_F. The expression for the momentum transfer in Eq. (2.24) clearly demonstrates its correspondence to electrons scattering off the domain wall: it increases for increasing reflection and decreases for increasing transmission.

The explicit form of the spin-transfer torque F_ϕ has $\propto T_{\downarrow\uparrow}$ as leading term, which is a measure for the number of electrons that follow the domain-wall magnetization.

The reflection and transmission coefficients are obtained by solving the Schrödinger equation of the system numerically, and matching the results to the asymptotic behavior in Eq. (2.20). As an example, we present the coefficients for $\Delta/2\varepsilon_F = 0.8$ as a function of $k_F\lambda$ in Fig. 2.3.

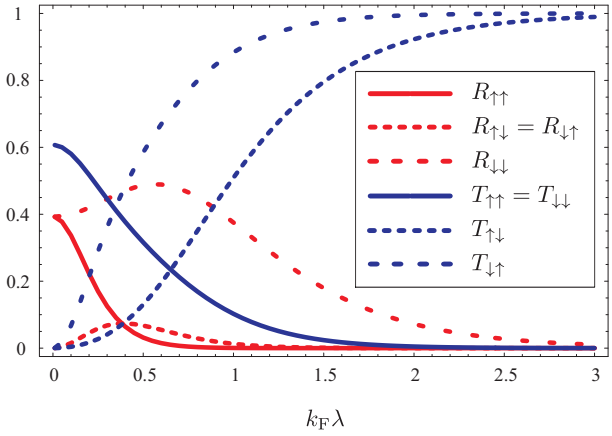

Figure 2.3: (color online). Transmission and reflection coefficients as functions of $k_F\lambda$ for $\Delta/2\varepsilon_F = 0.8$ and $V = 0$.

2.3 Results

As we have shown in the previous section, we are able to express Eqs. (2.14–2.17) in terms of transmission and reflection coefficients using Landauer-Büttiker transport, like in Eq. (2.24). As indicated, these coefficients are obtained by numerically solving the Schrödinger equation.

In the limit of vanishing voltage, Eq. (2.24) is the exact expression for the momentum transfer. In fact, the momentum transfer as well as the spin-transfer torque are for small $|e|V/\varepsilon_F$ proportional to the voltage, in agreement with the fact that these quantities are usually described as linear with the spin current [11]. We present the ratio of

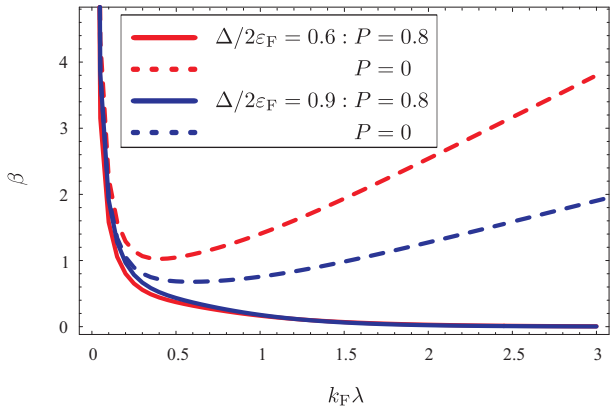

Figure 2.4: (color online). The parameter $\beta = F_X/F_\phi$ as a function of $k_F\lambda$ for $\Delta/2\varepsilon_F = 0.6$ and $\Delta/2\varepsilon_F = 0.9$, both at zero voltage. The dashed curves are obtained by ignoring polarization, the solid lines are obtained for a polarization of $P = 0.8$.

these forces that measures the degree of nonadiabaticity, denoted[1] by $F_X/F_\phi = \beta$, as a function of $k_F\lambda$ for several values $\Delta/2\varepsilon_F$ in Fig. 2.4.

In Fig. 2.4, the dashed curves show the result obtained directly from Eq. (2.24) and an equivalent expression for F_ϕ. We see that β is large for small $k_F\lambda$, as expected. The ratio, however, does not vanish for large $k_F\lambda$, which one would expect, but instead acquires a linear dependence on $k_F\lambda$. Mathematically, this is caused not by an increase of momentum transfer, but instead by a vanishing spin transfer. We can make sure that the spin transfer does not vanish by taking into account the polarization of the incoming electron current [40, 41]. If we do take this into account, such that $R_{\sigma\uparrow} \to R_{\sigma\uparrow}(1+P)$, $R_{\sigma\downarrow} \to R_{\sigma\downarrow}(1-P)$, and equivalently for transmission coefficients, we find for $P = 0.8$ the solid curves in Fig. 2.4. We see that these curves indeed go to zero in the adiabatic limit $k_F\lambda \gg 1$. From Fig. 2.4, it is clear that the polarization plays a big role from values $k_F\lambda \simeq 0.3$ onwards. Note that our theory does not take into account the dissipative spin-transfer torque, which gives similar contributions as momentum transfer [9].

For the damping parameters α_X and α_ϕ, we find that for small $|e|V/\varepsilon_F$, they both acquire corrections linear in the voltage, in agreement with Katsura *et al.* [42] and Núñez and Duine [35]. The dependence on $k_F\lambda$ is much less trivial, as is shown in

[1] Note that this β is not the parameter for the dissipative spin-transfer torque. However, since it enters the equations of motion in Eq. (2.13) in the same way as the dissipative spin-transfer torque, it is denoted by β.

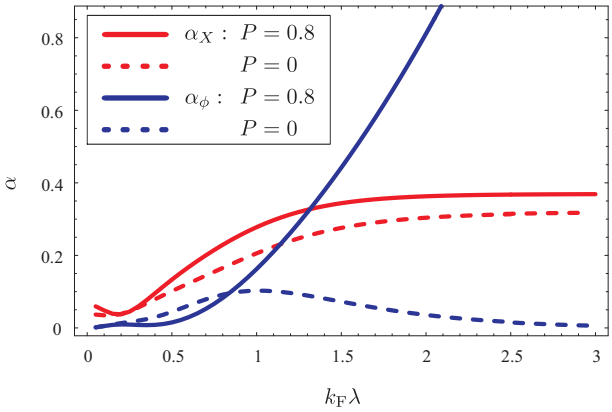

Figure 2.5: (color online). The damping parameters α_X and α_ϕ as a function of $k_F\lambda$ for $\Delta/2\varepsilon_F = 0.9$, both at zero voltage. The dashed curves are obtained by ignoring polarization, the solid lines are obtained for a polarization of $P = 0.8$.

Fig. 2.5, where the curves are taken at zero voltage.

The unpredictable behavior of the damping parameters as a function of $k_F\lambda$ for small $k_F\lambda$ arises from the details of the solutions of the Schrödinger equation. For large $k_F\lambda$, we see that without polarization α_ϕ goes to zero, whereas for nonzero polarization, it increases quadratically. This is understood from the fact that damping in the angle ϕ arises from emission of spin waves. This in its turn is closely related to spin-transfer torque, which goes to zero for $P = 0$ but assumes nonzero values for $P > 0$, as was discussed earlier in this section. It should be noted, however, that this approach breaks down for large values $k_F\lambda$ since we then lose phase coherence as $\lambda > L_\phi$. Furthermore, the polarization could be addressed in a more rigorous way by taking into account more transverse channels. Note that the fact that $\alpha_X \neq \alpha_\phi$ is a specific example of inhomogeneous damping as discussed by Foros *et al.* [37].

The effective temperatures of the system depend on the dimensionless parameters $k_F\lambda$ and $\Delta/2\varepsilon_F$. In Fig. 2.6 we show the effective temperatures for X and ϕ as functions of $|e|V/k_BT$ for $k_F\lambda = 1$ and several values $\Delta/2\varepsilon_F$. The solid curves are obtained for $P = 0.6$, the dashed curves do not take into account polarization. Note that the effective temperatures due to current-induced fluctuations can be substantially larger than the actual temperature, and are for large voltage proportional to $|e|V$.

As an application of the effective temperatures derived above, we compute depinning times as a function of the voltage. The effective temperature $T_{\mathrm{eff,X}}$ influences depinning from a spatial potential for the domain wall, such as a nanocon-

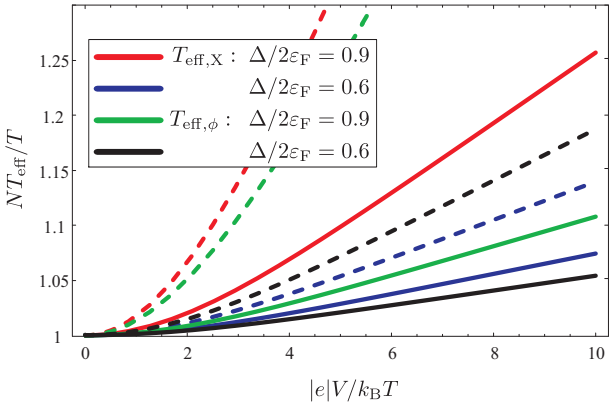

Figure 2.6: (color online). The effective temperatures $NT_{\mathrm{eff},X}/T$ and $NT_{\mathrm{eff},\phi}/T$ as a function of $|e|V/k_{\mathrm{B}}T$ for $\Delta/2\varepsilon_{\mathrm{F}} = 0.6$ or $\Delta/2\varepsilon_{\mathrm{F}} = 0.9$, all at $k_{\mathbf{F}}\lambda = 1$. The dashed curves are for $P = 0$, the solid curves are for $P = 0.6$.

striction. We model the pinning potential by a potential well of width 2ξ, given by $V = \Delta V(X^2/\xi^2 - 1)\theta(|X| - \xi)$ [11]. Using Arrhenius' law, the escape time is given by $\log(\tau\nu_0) = N(\Delta V - \hbar F_X \xi/\lambda)/k_{\mathrm{B}}T_{\mathrm{eff,X}}$, where $\nu_0 \sim \Delta V/\hbar$ is the attempt frequency. Note that the effect of the momentum transfer is determined by the ratio $\xi/\Delta V$, and that the force itself is still dependent on the number of spins N. We show our results for $\Delta V\lambda/\xi = 1$ meV, $N = 10$ and several temperatures in Fig. 2.7. The results for $T_{\mathrm{eff}} = T$ are also shown. Note that current-induced fluctuations decrease depinning times with respect to the result with the actual temperature. Note that we did not take into account polarization, which reduces this effect since polarization brings down the effective temperature, as was seen in Fig. 2.6.

2.4 Discussion and conclusion

We have established a microscopic theory that describes the effects of current-induced fluctuations on a domain wall. Since fluctuations in the current influence the system via spin transfer and momentum transfer, we find two separate forces, dampings and effective temperatures that correspond to these processes. We note that the ratio of the momentum transfer and the spin transfer $\beta = F_X/F_\phi$ that we calculate does not yet include the contribution due to spin relaxation, *i.e.*, the β discussed in Chapter 1. However, when the domain wall is narrow, this contribution is small compared to the contribution due to momentum transfer and can therefore be ignored. In addition to

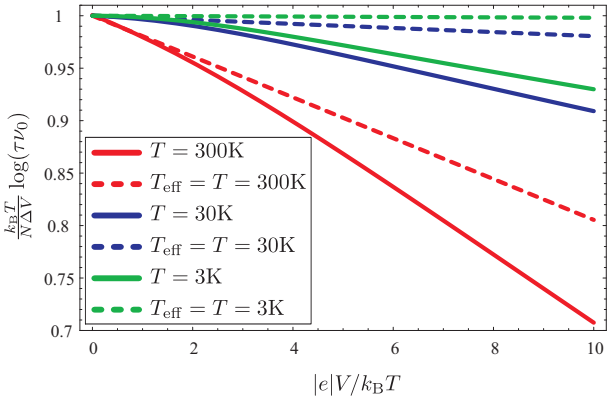

Figure 2.7: (color online). Logarithm of the escape time $(k_B T/N\Delta V)\log\tau\nu_0$ as a function of $|e|V/k_B T$ with (solid curves) and without (dashed curves) current-induced fluctuations. We used $\Delta V\lambda/\xi = 1$ meV, $N = 10$, $k_F\lambda = 1$, $\Delta = \varepsilon_F$, $P = 0$, and several temperatures.

the contribution due to the coupling of the domain wall with the electrons in the leads, that we consider here, there is an intrinsic contribution to the damping due to spin-relaxation, which is of the order $\alpha_0 \sim 0.01 - 0.1$ (this is the damping in Eq. (1.1)) in bulk materials, *i.e.*, of the same order as the voltage-dependent damping parameters that we obtain. A voltage-independent contribution to the damping will decrease the effective temperature, and thereby increase the depinning time somewhat.

As an application, we have studied depinning of the domain wall from a nanoconstriction. The width of the domain wall in nanocontacts is approximately the same as the nanocontact itself [31]. In experiments, it can be as small as $\lambda \sim 1$ nm [32, 33], which is smaller than the phase coherence length $L_\phi \sim 10$ nm in metals at room temperature and therefore permits a Landauer-Büttiker transport approach. Tatara *et al.* [43] have shown that in nanocontacts in metals Ni and Co, the exchange-splitting energy can reach high values $\Delta/2\varepsilon_F \simeq 0.98$. The voltage on the system in the experiment by Coey *et al.* [44] is of the order $|e|V \sim 0.1$ eV, which leads to $|e|V/k_B T \simeq 4$ at room temperature. The potential barrier in experiments on nanocontacts for typical displacements $\xi \sim 10\lambda$ [32] is very large $\Delta V \sim 10$ eV, but can be tuned by applying an external magnetic field. We see from Fig. 2.7 that at room temperature, the current-induced fluctuations already have an effect on depinning times, even if we take into account the fact that polarization might reduce this effect somewhat. At lower temperatures, this effect becomes larger. Under these circumstances, Coey *et al.* [44] find no evidence for heating effects, which would be another source of increased fluctuations. Therefore, current-induced fluctuations should be observable with domain walls in

nanocontacts.

Depinning of the angle ϕ is possible for relatively low values of the transverse anisotropy $K_\perp$. This depinning corresponds to switching between Néel walls of different chirality. Between the Néel wall configurations, the domain wall takes the form of a Bloch wall, that has higher energy. Coey *et al.* [44] have argued that in nanoconstrictions, the energy difference is comparable to the thermal energy at room temperature. Now, $T_{\mathrm{eff},\phi}$ is the effective temperature of interest, and from Fig. 2.6 we observe that current-induced fluctuations substantially alter this temperature. We therefore expect that effects of current-induced fluctuations on fluctuation-assisted domain-wall transformations can be significant.

Chapter 3

Current fluctuations due to Brownian motion of domain walls

Abstract

We compute the power spectrum of the noise in the current due to spin motive forces by a fluctuating domain wall. We find that the power spectrum of the noise in the current is colored, and depends on the Gilbert damping, the spin-transfer torque parameter β, and the domain-wall pinning potential and magnetic anisotropy. We also determine the average current induced by the thermally-assisted motion of a domain wall that is driven by an external magnetic field. Our results suggest that measuring the power spectrum of the noise in the current in the presence of a domain wall may provide a new method for characterizing the current-to-domain-wall coupling in the system.

3.1 Introduction

Voltage noise has long been considered a problem. Engineers have been concerned with bringing down noise in electric circuits for more than a century. The seminal work by Johnson [45] and Nyquist [46] on noise caused by thermal agitation of electric charge carriers (nowadays called Johnson-Nyquist noise) was largely inspired by the problem caused by noise in telephone wires. The experimental work by Johnson tested the earlier observations by engineers that noise increases with increasing resistance in the circuit and increasing temperature. He was able to show that there would always be a minimal amount of noise, beyond which reduction of the noise is not possible, thus providing a very practical tool for people working in the field. At the same time, the theoretical support for these predictions was given by Nyquist. It is probably not a coincidence that, at the time of his research, Nyquist worked for the American Telephone and Telegraph Company.

As long as noise is frequency-independent, *i.e.*, white like Johnson-Nyquist noise, it is indeed often little more than a nuisance (a notable exception to this is shot noise [22] at large bias voltage). However, frequency-dependent, *i.e.*, colored noise can contain interesting information on the system at hand. For example, in a recent paper Xiao *et al.* [47] show that, via the mechanism of spin pumping [48], a thermally agitated spin valve emits noisy currents with a colored power spectrum. They show that the peaks in the spectrum coincide with the precession frequency of the free ferromagnet of the spin valve. This opens up the possibility of an alternative measurement of the ferromagnetic resonance frequencies and damping, where one does not need to excite the system, but only needs to measure the voltage-noise power spectrum. Here, we see that properties of the noise contain information on the system. Clearly, this proposal only works if the Johnson-Nyquist noise is not too large compared to the colored noise.

Not only precessing magnets in layered structures induce currents: As we have seen in Chapter 1, recent theoretical work has increased interest in the inverse effect of current-driven domain-wall motion, whereby a moving domain wall induces an electric current [12–16]. Experimentally, this effect has been seen recently with field-driven domain walls in permalloy wires [20]. These spin motive forces ultimately arise from the same mechanism as spin pumping induced by the precessing magnet in a spin valve, *i.e.*, both involve dynamic magnetization that induces spin currents that are subsequently converted into a charge current.

In this chapter, we study the currents induced by domain walls at nonzero temperature. In particular, we determine the (colored) power spectrum of the emitted currents due to a fluctuating domain wall, both in the case of an unpinned domain wall, and in the case of a domain wall that is extrinsically pinned. We also compute the average current induced by a field-driven domain wall at nonzero temperature. We end with a short discussion and, in particular, compare the magnitude of the colored noise obtained by us with the magnitude of the Johnson-Nyquist noise.

3.2 Spin motive forces due to fluctuating domain walls

In this section, we compute the power spectrum of current fluctuations due to spin motive forces that arise when a domain wall is thermally fluctuating. We consider separately the case of intrinsic and extrinsic pinning.

3.2.1 Model and approach

The equations of motion for the position X and the chirality ϕ of a rigid domain wall at nonzero temperature are given by (we use Eq. (1.14) with $j = 0$ and $H_{\text{ext}} = 0$)[11, 17, 18]

$$\frac{\dot{X}}{\lambda} = \alpha\dot{\phi} + \frac{K_\perp}{\hbar}\sin(2\phi) + \eta_1 \,, \tag{3.1}$$

$$\dot{\phi} = -\alpha\frac{\dot{X}}{\lambda} + F_{\text{pin}} + \eta_2 \,, \tag{3.2}$$

where α is Gilbert damping, $K_\perp$ is the hard-axis anisotropy, and $\lambda = \sqrt{K_{\text{easy}}/J}$ is the domain-wall width, with J the spin stiffness and K_{easy} the easy-axis anisotropy. We introduce a pinning force, denoted by $F_{\text{pin}} = (\lambda/\hbar)\partial V_{\text{ext}}/\partial X$, to account for irregularities in the material. We have assumed that the pinning potential only depends on the position of the domain wall. Pinning sites turn out to be well-described by a potential that is quadratic in X, such that we can take $F_{\text{pin}} = -2\omega_{\text{pin}}X/\lambda$ [11]. As mentioned before, the Gaussian stochastic forces η_i describe thermal fluctuations and obey the fluctuation-dissipation theorem

$$\langle\eta_i(t)\rangle = 0 \,; \qquad \langle\eta_i(t)\eta_j(t')\rangle = \frac{2\alpha k_{\text{B}}T}{\hbar N}\delta_{i,j}\delta(t-t') \,. \tag{3.3}$$

Note that in this expression, the temperature T is effectively reduced by the number of magnetic moments in the domain wall $N = 2\lambda A/a^3$, with A the cross-sectional area of the sample, and a the lattice spacing. Up to linear order in the coordinate ϕ, valid when $K_\perp > k_{\text{B}}T$, we can write the equations of motion in Eqs. (3.1) and (3.2) as

$$\partial_t\vec{x} = M\vec{x} + N\vec{\eta} \,, \tag{3.4}$$

where

$$M = \frac{2}{1+\alpha^2}\begin{pmatrix} -\alpha\omega_{\text{pin}} & \frac{K_\perp}{\hbar} \\ -\omega_{\text{pin}} & -\alpha\frac{K_\perp}{\hbar} \end{pmatrix} \,; \quad \vec{x} = \begin{pmatrix} \frac{X}{\lambda} \\ \phi \end{pmatrix} \,, \tag{3.5}$$

and

$$N = \frac{1}{1+\alpha^2}\begin{pmatrix} 1 & \alpha \\ -\alpha & 1 \end{pmatrix} \,; \quad \vec{\eta} = \begin{pmatrix} \eta_1 \\ \eta_2 \end{pmatrix} \,. \tag{3.6}$$

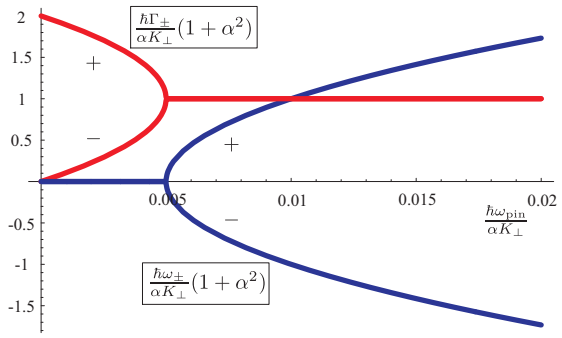

Figure 3.1: Values of $\Gamma_\pm$ (red curves) and $\omega_\pm$ (blue curves) as a function of the pinning for $\alpha = 0.02$.

We readily find that the eigenfrequencies of the system, determined by the eigenvalues $\Lambda_\pm$ of the matrix M, are

$$\Lambda_\pm \equiv i\omega_\pm - \Gamma_\mp = -\frac{\alpha}{1+\alpha^2}\left(\omega_{\rm pin} + \frac{K_\perp}{\hbar}\right) \pm \frac{\alpha}{1+\alpha^2}\sqrt{\left(\omega_{\rm pin} - \frac{K_\perp}{\hbar}\right)^2 - \frac{4}{\alpha^2}\omega_{\rm pin}\frac{K_\perp}{\hbar}}\,, \tag{3.7}$$

with both the eigenfrequencies $\omega_\pm$ and their damping rates $\Gamma_\pm$ real numbers. Their behavior as a function of $\hbar\omega_{\rm pin}/K_\perp$ is shown in Fig. 3.1. Note that this expression has an imaginary part for pinning potentials that obey $\hbar\omega_{\rm pin}/K_\perp \geq (\alpha/2)^2$, and, because for typical materials the damping assumes values $\alpha \sim 0.01 - 0.1$, the eigenfrequency assumes nonzero values already for very small pinning potentials. Without pinning potential ($\omega_{\rm pin} = 0$) the eigenvalues are purely real-valued and the motion of the domain wall is overdamped since $\Gamma_\pm \geq 0$ and $\omega_\pm = 0$.

If we include temperature, we find from the solution of Eq. (3.4) [without loss of generality we choose $X(t=0) = \phi(t=0) = 0$] that the time derivatives of the collective coordinates are given by

$$\partial_t \vec{x}(t) = Me^{Mt}\int_0^t dt' e^{-Mt'} N\vec{\eta}(t') + N\vec{\eta}(t)\,, \tag{3.8}$$

for one realization of the noise. By averaging this solution over realizations of the noise, we compute the power spectrum of the current induced by the domain wall under the influence of thermal fluctuations as follows.

It was shown by one of us [15] that up to linear order in time derivatives, the current induced by a moving domain wall is given by

$$I(t) = -\frac{A\hbar}{|e|L}(\sigma_\uparrow - \sigma_\downarrow)\left[\dot{\phi}(t) - \beta\frac{\dot{X}(t)}{\lambda}\right], \tag{3.9}$$

with L the length of the sample, and β the sum of the phenomenological dissipative spin-transfer torque parameter [9] and non-adiabatic contributions. The power spectrum is defined as

$$P(\omega) = 2\int_{-\infty}^{+\infty} d(t-t')e^{-i\omega(t-t')}\langle I(t)I(t')\rangle . \tag{3.10}$$

Note that in this definition the power spectrum has units $[P] = \mathrm{A}^2/\mathrm{Hz}$, not to be mistaken with the power spectrum of a voltage-voltage correlation, which has units $[P] = \mathrm{V}^2/\mathrm{Hz}$. In both cases, however, the power spectrum can be seen as a measure of the energy output per frequency interval. We introduce now the matrix

$$O = \left(\frac{A\hbar}{|e|L}\right)^2(\sigma_\uparrow - \sigma_\downarrow)^2\begin{pmatrix}\beta^2 & -\beta\\ -\beta & 1\end{pmatrix}, \tag{3.11}$$

so that we can write the correlations of the current as

$$\begin{aligned}
&\langle I(t)I(t')\rangle = \left\langle [\partial_t\vec{x}(t)]^{\mathrm{T}} O\partial_{t'}\vec{x}(t')\right\rangle = \\
&\int_0^t\int_0^{t'} dt''dt'''\left\langle \vec{\eta}(t'')^{\mathrm{T}}N^{\mathrm{T}}e^{M^{\mathrm{T}}(t-t'')}M^{\mathrm{T}}OMe^{M(t'-t''')}N\vec{\eta}(t''')\right\rangle \\
&+\int_0^t dt''\left\langle \vec{\eta}(t'')^{\mathrm{T}}N^{\mathrm{T}}e^{M^{\mathrm{T}}(t-t'')}M^{\mathrm{T}}ON\vec{\eta}(t')\right\rangle \\
&+\int_0^{t'} dt''\left\langle \vec{\eta}(t)^{\mathrm{T}}N^{\mathrm{T}}OMe^{M(t'-t'')}N\vec{\eta}(t'')\right\rangle + \left\langle \vec{\eta}(t)^{\mathrm{T}}N^{\mathrm{T}}ON\vec{\eta}(t')\right\rangle = \\
&\frac{\alpha k_{\mathrm{B}}T}{\hbar N}\theta(t-t')\left\{\int_0^{t'} dt''\mathrm{Tr}\left[N^{\mathrm{T}}e^{M^{\mathrm{T}}(t-t'')}M^{\mathrm{T}}OMe^{M(t'-t'')}N\right]\right. \\
&\qquad\left. +\mathrm{Tr}\left[N^{\mathrm{T}}e^{M^{\mathrm{T}}(t-t')}M^{\mathrm{T}}ON\right]\right\} \\
&+\frac{\alpha k_{\mathrm{B}}T}{\hbar N}\theta(t'-t)\left\{\int_0^{t} dt''\mathrm{Tr}\left[N^{\mathrm{T}}e^{M^{\mathrm{T}}(t-t'')}M^{\mathrm{T}}OMe^{M(t'-t'')}N\right]\right. \\
&\qquad\left. +\mathrm{Tr}\left[N^{\mathrm{T}}OMe^{M(t'-t)}N\right]\right\} + \frac{\alpha k_{\mathrm{B}}T}{\hbar N}\delta(t-t')\mathrm{Tr}\left[N^{\mathrm{T}}ON\right] .
\end{aligned} \tag{3.12}$$

We evaluate the traces that appear in this expression to find that the power spectrum is given by

$$
\begin{aligned}
&P(\omega) = \\
&2\left(\frac{A\hbar}{|e|L}\right)^2 \frac{(\sigma_\uparrow-\sigma_\downarrow)^2}{1+\alpha^2}\frac{\alpha k_{\rm B}T}{\hbar N}\times\Bigg[(1+\beta)^2-\Bigg\{(1+\beta^2)(1+\alpha^2)^2\left(\frac{\hbar\omega_{\rm pin}}{K_\perp}\right)^2 \\
&-\left[\beta^2-\alpha^2+2(1+\beta^2)\frac{\hbar\omega_{\rm pin}}{K_\perp}+(1-\alpha^2\beta^2)\left(\frac{\hbar\omega_{\rm pin}}{K_\perp}\right)^2\right]\left(\frac{\hbar\omega}{K_\perp}\frac{1+\alpha^2}{2}\right)^2\Bigg\}\Big/ \\
&\Bigg\{(1+\alpha^2)^2\left(\frac{\hbar\omega_{\rm pin}}{K_\perp}\right)^2+\left[\alpha^2-2\frac{\hbar\omega_{\rm pin}}{K_\perp}+\alpha^2\left(\frac{\hbar\omega_{\rm pin}}{K_\perp}\right)^2\right]\left(\frac{\hbar\omega}{K_\perp}\frac{1+\alpha^2}{2}\right)^2 \\
&+\left(\frac{\hbar\omega}{K_\perp}\frac{1+\alpha^2}{2}\right)^4\Bigg\}\Bigg]\,. \qquad (3.13)
\end{aligned}
$$

3.2.2 Domain wall without extrinsic pinning

We first consider a domain wall with $F_{\rm pin}=0$. In this case, only the chirality ϕ determines the energy, a situation referred to as intrinsic pinning [11]. From the result in Eq. (3.13) we find that the power spectrum is given by

$$
\begin{aligned}
P(\omega) &= 2\left(\frac{A\hbar}{|e|L}\right)^2\frac{(\sigma_\uparrow-\sigma_\downarrow)^2}{1+\alpha^2}\frac{\alpha k_{\rm B}T}{\hbar N}\times \\
&\left\{(1+\beta)^2+\frac{\beta^2-\alpha^2}{\alpha^2}\left[1+\left(\frac{\hbar\omega}{K_\perp}\frac{1+\alpha^2}{2\alpha}\right)^2\right]^{-1}\right\}. \qquad (3.14)
\end{aligned}
$$

Indeed, we find that next to a constant contribution there is also a frequency-dependent contribution for $\beta\neq\alpha$, *i.e.*, the power spectrum is colored. The fact that $\beta=\alpha$ is a special case is understood from the fact that in that case we have macroscopic Galilean invariance. This translates to white noise in the current correlations. The power spectrum is a Lorentzian, centered around $\omega=0$ because the domain wall is overdamped in this case, with a width determined by the damping rate in Eq. (3.7) as $\hbar\Gamma_+/K_\perp = 2\alpha/(1+\alpha^2)$. Relative to the white-noise contribution

$$
P_{\rm W} = 2(1+\beta)^2\left(\frac{A\hbar}{|e|L}\right)^2\frac{(\sigma_\uparrow-\sigma_\downarrow)^2}{1+\alpha^2}\frac{\alpha k_{\rm B}T}{\hbar N}\,, \qquad (3.15)
$$

the height of the peak is given by $\Delta P = P_{\rm W}(\beta^2-\alpha^2)/\alpha^2$. The behavior of the power spectrum is illustrated in Fig. 3.2 for several values of β/α.

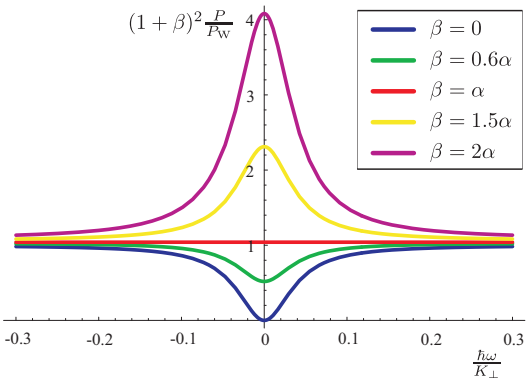

Figure 3.2: The power spectrum for $\alpha = 0.02$ and several values of β.

3.2.3 Extrinsically pinned domain wall

For extrinsically pinned domain walls the behavior of the power spectrum given by Eq. (3.13) is depicted in Fig. 3.3. We see that for $\hbar\omega_{\rm pin}/K_\perp \gtrsim \alpha^2$ the peaks in the power spectrum are approximately centered around the eigenfrequencies $\hbar\omega/K_\perp \simeq \pm 2\sqrt{\hbar\omega_{\rm pin}/K_\perp}$, consistent with Eq. (3.7). We can discern between two regimes, one where $\beta \sim \alpha$ in Figs. 3.3 (a-d), and one where $\beta \gg \alpha$ in Figs. 3.3 (e-f). In the former regime, the height of the peaks in the power spectrum depend strongly on the pinning. For small $\omega_{\rm pin}$ we see a clear dependence on the value of β, whereas for large $\omega_{\rm pin}$ this dependence is less significant. In the regime of large β, the height of the peaks hardly depends on the pinning and is approximately given by $P \simeq P_{\rm W}\beta^2/\alpha^2$. Note that the width of the peaks is independent of β. For pinning potentials $\alpha^2 < \hbar\omega_{\rm pin}/K_\perp$ the width is given by $\hbar\Gamma/K_\perp = \alpha(1+\hbar\omega_{\rm pin}/K_\perp)/(1+\alpha^2)$, so for $\hbar\omega_{\rm pin} \ll K_\perp$ the dependence of the width on the pinning is negligible.

3.3 Spin motive forces due to thermally-assisted field-driven domain walls

In this section we compute the average current that is induced by a moving domain wall. The domain wall is moved by applying an external magnetic field parallel to the easy axis of the sample. In this section we take into account temperature but ignore extrinsic pinning (see Ref. [49] for a calculation of spin motive forces in a weakly extrinsically pinned system for $\beta = 0$). The equations of motion for a field-driven

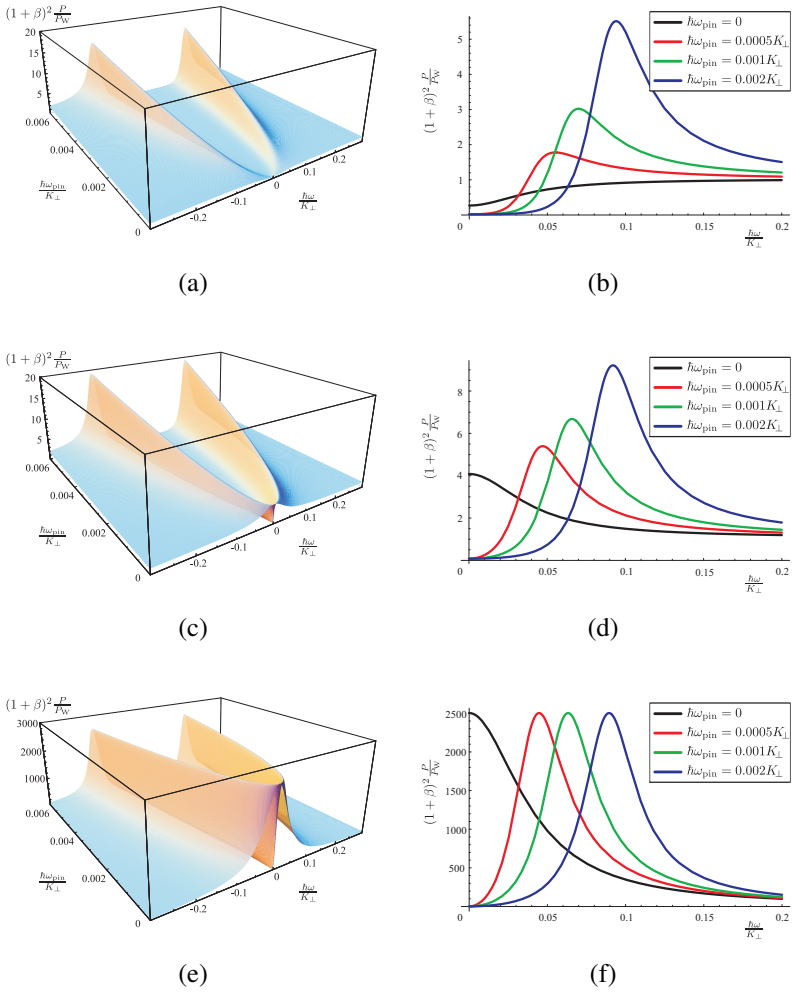

Figure 3.3: The power spectrum as a function of the frequency ω and the pinning potential $\omega_{\rm pin}$ for $\beta = \alpha/2$ (a,b), $\beta = 2\alpha$ (c,d) and $\beta = 50\alpha$ (e,f), all for $\alpha = 0.02$. Figs. (b,d,f) are slices taken from the 3D curves in Figs. (a,c,e), respectively.

domain wall are then given (compare Eq. (1.14)) by [11, 17, 18]

$$\frac{\dot{X}}{\lambda} = \alpha\dot{\phi} + \frac{K_\perp}{\hbar}\sin 2\phi + \eta_1 \,, \tag{3.16}$$

$$\dot{\phi} = -\alpha\frac{\dot{X}}{\lambda} + \frac{g\mu_{\rm B}B_z}{\hbar} + \eta_2 \,, \tag{3.17}$$

where gB_z is the magnetic field in the z-direction, and the stochastic forces are determined by Eq. (3.3). In earlier work [18], we computed from these coupled equations the average drift velocity of a domain wall (here, we set the applied spin current zero)

$$\alpha\frac{\langle\dot{X}\rangle}{\lambda} = -\langle\dot{\phi}\rangle + \frac{g\mu_{\rm B}B_z}{\hbar} \,, \tag{3.18}$$

with (we omit factors $1+\alpha^2 \simeq 1$)

$$\begin{aligned}\langle\dot{\phi}\rangle = -2\pi\frac{\alpha k_{\rm B}T}{\hbar N}\big(e^{-2\pi\frac{g\mu_{\rm B}B_zN}{\alpha k_{\rm B}T}}-1\big)\Big/ \\ \Bigg\{\int_0^{2\pi}d\phi e^{\frac{N}{k_{\rm B}T}\left(\frac{g\mu_{\rm B}B_z}{\alpha}\phi+\frac{K_\perp}{2}\cos 2\phi\right)}\Bigg[\int_0^{2\pi}d\phi' e^{-\frac{N}{k_{\rm B}T}\left(\frac{g\mu_{\rm B}B_z}{\alpha}\phi'+\frac{K_\perp}{2}\cos 2\phi'\right)} \\ +\big(e^{-2\pi\frac{g\mu_{\rm B}B_zN}{\alpha k_{\rm B}T}}-1\big)\int_0^{\phi}d\phi' e^{-\frac{N_{\rm DW}}{k_{\rm B}T}\left(\frac{g\mu_{\rm B}B_z}{\alpha}\phi'+\frac{K_\perp}{2}\cos 2\phi'\right)}\Bigg]\Bigg\} \,.\end{aligned} \tag{3.19}$$

Combining Eqs. (3.9) and (3.18) gives us the average current straightforwardly

$$\langle I\rangle = -\frac{A\hbar}{\alpha|e|L}(\sigma_\uparrow-\sigma_\downarrow)\left[(\alpha+\beta)\langle\dot{\phi}\rangle - \beta\frac{g\mu_{\rm B}B_z}{\hbar}\right] \,. \tag{3.20}$$

We evaluate this expression for several temperatures in Fig. 3.4. The black curve in Fig. 3.4 is computed at zero temperature. It increases linearly with the field up to the Walker-breakdown field $B_{\rm W} = \alpha K_\perp/g\mu_{\rm B}$, where it reaches a maximum current of $\langle I\rangle|e|L/Ag\mu_{\rm B}B_{\rm W}(\sigma_\uparrow-\sigma_\downarrow) = \beta/\alpha$. Then, it drops and even changes sign. This curve is consistent with the curves obtained by one of us [15]. There, an open circuit is treated where there is no current but a voltage. The voltage is related to the current as $\Delta V = \langle I\rangle L/A(\sigma_\uparrow+\sigma_\downarrow)$, such that indeed $\Delta V/V_0 = \langle I\rangle|e|L/Ag\mu_{\rm B}B_{\rm W}(\sigma_\uparrow-\sigma_\downarrow)$, where the normalization is defined as $V_0 = \mathcal{P}g\mu_{\rm B}B_{\rm W}/|e|$ and the polarization is given by $\mathcal{P} \equiv (\sigma_\uparrow-\sigma_\downarrow)/(\sigma_\uparrow+\sigma_\downarrow)$. Increasing temperatures smoothen the peak around the Walker-breakdown field, and for high temperatures, the peak vanishes altogether. Therefore, for fields smaller than the Walker-breakdown field and for small temperatures, the thermal fluctuations tend to decrease the average induced current. However, for higher temperatures, the current reverses and increases again. For fields sufficiently larger than the Walker-breakdown field, we always find a slight increase of the current as a function of temperature.

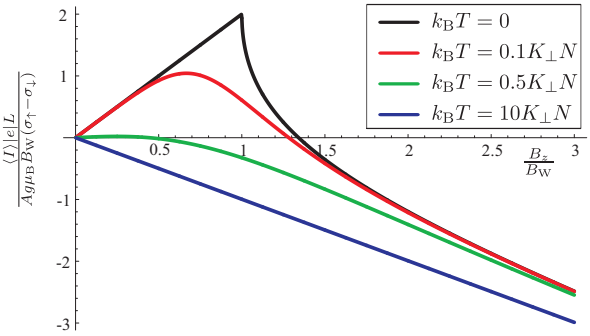

Figure 3.4: The average current induced by a domain wall as a function of the magnetic field applied to this domain wall. We show curves for several temperatures, with $\alpha = 0.02$ and $\beta = 2\alpha$. The normalization of the axes B_W is the Walker-breakdown field which is given by $B_W = \alpha K_\perp / g\mu_B$.

3.4 Discussion and conclusion

In Section 3.2 we computed power spectra for domain walls, both with and without extrinsic pinning. In ferromagnetic metals, the spin-transfer torque parameter has values $\beta \sim \alpha$, for which we see that for large pinning $\hbar\omega_{\text{pin}}/K_\perp \gtrsim \alpha^2$ the power spectra only weakly depend on the spin-transfer torque parameter β. Therefore, determination of β is only possible for very small pinning potentials. In an ideally clean sample without extrinsic pinning the height and sign of the peak in the power spectrum can give a clear indication whether β is smaller, (approximately) equal, or larger than α.

In order to perform these experiments, the contributions due to the domain wall should not be completely overwhelmed by Johnson-Nyquist noise. The ratio of the peaks in our power spectrum and the Johnson-Nyquist noise determine the resolution of the experiment, and we want it to be at least of the order of a percent. We use that the resistance of the domain wall is small, and the Johnson-Nyquist noise is governed by the resistance of the wire. For a wire of length L and cross-section A, the power spectrum due to Johnson-Nyquist noise is given by $P_{\text{JN}} = 4k_BT(\sigma_\uparrow + \sigma_\downarrow)A/L$. From Section 3.2.2 we can estimate the ratio of the height of the peak and the Johnson-Nyquist noise as $\Delta P/P_{\text{JN}} \simeq [(\beta/\alpha)^2 - 1]\alpha A\hbar(\sigma_\uparrow + \sigma_\downarrow)/(4LN\mathcal{P}^2e^2)$. To make a rough estimate of this ratio, we use $\lambda \simeq 20$nm such that $A/N \simeq 2 \cdot 10^{-2}\text{Å}^2$ for $a \simeq 2$Å, a polarization $\mathcal{P} \simeq 0.7$ and a conductivity $\sigma_\uparrow + \sigma_\downarrow \simeq 10^7\text{A/Vm}$. We then find $\Delta P/P_{\text{JN}} \simeq 10^{-2}\text{Å}/L$, which shows that the wire length must satisfy $L < 1$Å in order to have a

resolution of 1%. We therefore conclude that this effect at zero pinning is impossible to see in experiment, where wires are typically at least of the order of $L \simeq 10\mu$m, *i.e.*, five orders of magnitude larger. We can try to increase the signal by turning on a pinning potential. Insertion of the eigenfrequencies $\omega_\pm$ from Eq. (3.7) in Eq. (3.13) shows us that we can maximally gain a factor $\alpha^{-2} \simeq 10^4$ for $\alpha = 0.01$, as illustrated in Fig. 3.5. We can also still gain some resolution by considering a domain wall in a

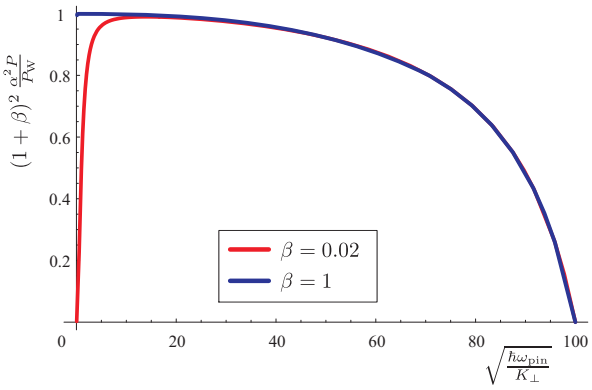

Figure 3.5: The height of the peaks in the power spectrum as a function of the pinning. We used $\alpha = 0.02$ and two values for β. We checked that the curves do not differ significantly for different values for α and therefore, the maximal value of the peaks in the power spectrum is $\Delta P(1+\beta^2)/P_{\rm JN} \simeq \alpha^{-2}$. Note that the dependence on β is negligible for large pinning. This curve was obtained by inserting the eigenfrequencies $\omega_\pm$ from Eq. (3.7) in the expression for the power spectrum in Eq. (3.13).

nanoconstriction, where the width can be as small as $\lambda = 1$nm [31]. All this adds up to a resolution of $\Delta P/P_{\rm JN} \sim 1\%$. Therefore, with all parameter values set to ideal values it appears to be possible to observe our predictions in ferromagnetic metals, although the experimental challenges are big.

In a magnetic semiconductor like GaMnAs the number of magnetic moments in the domain wall is two orders of magnitude smaller than in a ferromagnetic conductor. This increases the ratio $\Delta P/P_{\rm JN}$ with a factor 100. However, the conductivity is also considerably smaller than that in a ferromagnetic metal. The conductivity of GaMnAs depends on many parameters, but a reasonable estimate is that it is at least about three orders of magnitude smaller than that of a metal, although usually even smaller. Therefore, the advantage of a small number of magnetic moments is cancelled. Another property, however, of GaMnAs is that the parameter β can assume considerably higher values [50], up to $\beta = 1$. This does not influence the maximal value of the power spectrum, but it does dramatically increase the value for small pinning.

Note that there are contributions to the noise that we did not discuss in this article. For example, the time-dependent magnetic field caused by a moving domain wall will induce electric currents that contribute to the colored power spectrum. Distinguishing such contributions from the spin motive forces was essential for the experimental results by Yang *et al.* [20], and would also be important here.

In Sec. 3.3, we calculated the current induced by a field-driven domain wall under the influence of temperature. We estimate that in ferromagnetic metals at room temperature that $k_{\mathrm{B}}T/K_{\perp}N \simeq 10^{-3}$, which is indistinguishable from the zero-temperature curve in Fig. 3.4. However, for magnetic semiconductors, like GaMnAs, we find $k_{\mathrm{B}}T/K_{\perp}N \simeq 10^{-1}$ at $T = 100\mathrm{K}$, which corresponds to the red curve in Fig. 3.4. We therefore expect finite-temperature effects to be important in magnetic semiconductors like GaMnAs.

Chapter 4

Spin motive forces due to driven magnetic vortices

Abstract

We study spin motive forces, i.e., spin-dependent forces and voltages induced by time-dependent magnetization textures, for moving magnetic vortices and domain walls. First, we consider the voltage generated by a one-dimensional field-driven domain wall. Next, we perform detailed calculations on field-driven vortex domain walls. We find that the results for the voltage as a function of magnetic field differ between the one-dimensional and vortex domain wall. For the experimentally relevant case of a vortex domain wall, the dependence of voltage on field around Walker breakdown depends qualitatively on the ratio of the so-called β parameter to the Gilbert damping constant, and thus provides a way to determine this ratio experimentally. We also consider vortices on a magnetic disk in the presence of an AC magnetic field. In this case, the phase difference between field and voltage on the edge is determined by the β parameter, providing another experimental method to determine this quantity.

4.1 Introduction

One of the recent developments in spintronics is the study of spin motive forces [12] and spin pumping [48]. These effects lead to the generation of charge and spin currents due to time-dependent magnetization textures. As we have seen in Chapter 1, the idea of spin motive forces due to domain walls is easily understood on an intuitive level: if an applied current induces domain-wall motion [5–10], Onsager's reciprocity theorem tells us that a moving domain wall will induce a current. This idea was already put forward in the eighties by Berger [51]. In the case of a domain wall driven by large magnetic fields (*i.e.,* well above the so-called Walker breakdown field),

a fairly simple approach to the problem is justified where one goes to a frame of reference in which the spin quantization axis follows the magnetization texture [52, 53]. This transformation gives rise to a vector potential from which effective electric and magnetic fields are derived. Experimentally, the domain-wall induced voltage has recently been measured above Walker breakdown [20], and the results are consistent with this approach. It has also been shown that the induced voltage well above Walker breakdown is determined from a topological argument that follows from the properties of the above-mentioned vector potential [54].

The above approach only captures the reactive contribution to the spin-motive forces. When the velocity of the domain wall is below or just above Walker breakdown, a theory is needed that includes more contributions to the spin motive forces. Renewed interest has shed light on the non-adiabatic and dissipative contributions to the spin motive forces [13–15] that are important in this regime. In this chapter, we study this regime.

This chapter is organized as follows. In Section 4.2 we summarize earlier results that give a general framework to compute electrochemical potentials for given time-dependent magnetization textures. In Section 4.3 we consider an analytical model for a one-dimensional domain wall and numerically determine the form of the spin accumulation and the electrochemical potential. The results agree with the known results for the potential difference induced by a moving one-dimensional domain wall in Section 1.5 [15]. In Section 4.4 we turn to two-dimensional systems and study a vortex domain wall in a permalloy strip. We use a micro-magnetic simulator to obtain the magnetization dynamics, and numerically evaluate the reactive and dissipative contributions to the voltage below and just above Walker breakdown and compare with experiment [20]. Another example of a two-dimensional system is a vortex on a disk which we treat in Section 4.5. For small enough disks, the magnetic configuration is a vortex. Both experimentally and theoretically, it has been shown that a vortex driven by an oscillating magnetic field will rotate around its equilibrium position [55–57, 59, 77]. This gives rise to a voltage difference between the disk edge and center as was recently discussed by Ohe *et al.* [60]. Here, we extend this study by including both the reactive and the dissipative contributions to the voltage, that turn out to have a relative phase difference. This gives rise to a phase difference between the drive field and voltage that is determined by the β parameter.

4.2 Model

As we have seen in Section 1.4, the spin-motive force field $\mathbf{F}(\vec{x})$ induced by a time-dependent magnetization texture that is characterized at position $\vec{x}$ by a unit-vector

magnetization direction $\mathbf{\Omega}(\vec{x},t)$ is given by [14, 15]

$$F_i = \frac{\hbar}{2}\left[\mathbf{\Omega}\cdot(\partial_t\mathbf{\Omega}\times\nabla_i\mathbf{\Omega}) + \beta(\partial_t\mathbf{\Omega}\cdot\nabla_i\mathbf{\Omega})\right] . \tag{4.1}$$

This force field acts in this form on the majority spins, and with opposite sign on minority spins. In this expression, the first term is the well-known reactive term [12]. The second term describes dissipative effects due to spin relaxation [14, 15] and is proportional to the β parameter. The spin accumulation μ_s in the system follows from [14]

$$\frac{1}{\lambda_{sd}^2}\mu_s - \nabla^2\mu_s = -\boldsymbol{\nabla}\cdot\mathbf{F} , \tag{4.2}$$

where $\lambda_{sd} = \sqrt{\tau D}$ is the spin-diffusion length, with τ a characteristic spin-flip time and D the effective spin-diffusion constant. Here, we assume that the spin-relaxation time is much smaller than the timescale for magnetization dynamics. The total electrochemical potential μ that is generated by the spin accumulation due to a non-zero current polarization in the system is computed from [14]

$$-\nabla^2\mu = \mathcal{P}(\nabla^2\mu_s - \boldsymbol{\nabla}\cdot\mathbf{F}) , \tag{4.3}$$

where the current polarization is given by $\mathcal{P} = (\sigma_\uparrow - \sigma_\downarrow)/(\sigma_\uparrow + \sigma_\downarrow)$. Note that there is no charge accumulation for $\sigma_\uparrow = \sigma_\downarrow$, with $\sigma_\uparrow(\sigma_\downarrow)$ the conductivity of the majority (minority) spin electrons.

The magnetization dynamics is found from the Landau-Lifschitz-Gilbert equation (compare Eq. (1.1))

$$\frac{\partial\mathbf{\Omega}}{\partial t} = \mathbf{\Omega}\times\gamma\mathbf{H}_{\text{eff}} - \alpha\mathbf{\Omega}\times\frac{\partial\mathbf{\Omega}}{\partial t} . \tag{4.4}$$

Here, $\mathbf{H}_{\text{eff}}$ is the effective magnetic field that includes exchange interaction, anisotropy, and external field, and α is the Gilbert damping constant.

4.3 One-dimensional domain wall

For one-dimensional problems the voltage difference can be found easily. For example, an analytic expression for the electric current (which is the open-circuit equivalent of the chemical-potential difference) was obtained in Section 1.5 for an analytical model for a one-dimensional driven domain wall [15]. In this section, we solve the potential problem for a one-dimensional domain wall and obtain the explicit position dependence of the spin accumulation and the chemical potential.

A one-dimensional domain wall ($\partial_y \mathbf{\Omega} = \partial_z \mathbf{\Omega} = 0$) is described by[11]

$$\theta(x,t) = 2\arctan\left\{e^{Q[x-X(t)]/\lambda}\right\}, \qquad \phi(x,t) = 0\,, \tag{4.5}$$

with $\mathbf{\Omega} = (\sin\theta\cos\phi, \sin\theta\sin\phi, \cos\theta)$. Here, $Q = \pm 1$ is called the topological charge of the domain wall since it indicates the way in which an external field affects the domain-wall motion, *i.e.*, a field in the direction $+\hat{z}$ will move a domain wall in the direction $Q\hat{x}$. Note that in this section, we repeat computations from Section 1.5 to include the dependence on the topological charge Q.

To study the time evolution of a domain wall, we let $\phi(x) \to \phi_0(t)$ so that the wall is described by time-dependent collective coordinates $\{X(t), \phi_0(t)\}$, called position and chirality, respectively. For external fields smaller than the Walker-breakdown field, there is no domain-wall precession (*i.e.,* the chirality is constant), and the domain wall velocity v is constant so that $\partial_t \mathbf{\Omega} = -v\partial_x \mathbf{\Omega}$. Since $\partial_y \mathbf{\Omega} = \partial_z \mathbf{\Omega} = 0$, we immediately see that the first term on the right-hand side of Eq. (4.1) vanishes, and that the force is pointing along the x-axis. We then find that $F_x = (\beta v\hbar/2)/(\lambda^2 \cosh[x/\lambda]^2)$. Due to symmetry we have that $\partial_y \mu = \partial_z \mu = \partial_y \mu_s = \partial_z \mu_s = 0$. In Figs. 4.1 and 4.2 we plot the spin accumulation and the electrochemical potential as a function of x.

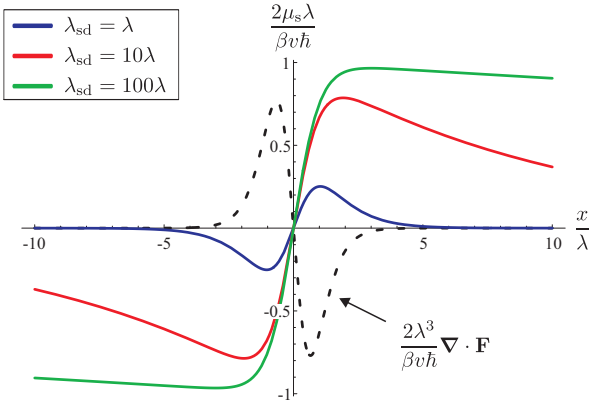

Figure 4.1: Spin accumulation as a function of position for several values of the spin-diffusion length. The black dotted line gives the value of the source term. The spin accumulation tends to zero for $x \to \pm\infty$.

From Fig. 4.2 we see that the total potential difference $\Delta\mu = \mu(x \to \infty) - \mu(x \to -\infty)$ is independent of the spin-diffusion length and linear in the parameter β: $\Delta\mu = \hbar\mathcal{P}\beta v/\lambda$. Note that this result is only valid below Walker Breakdown.

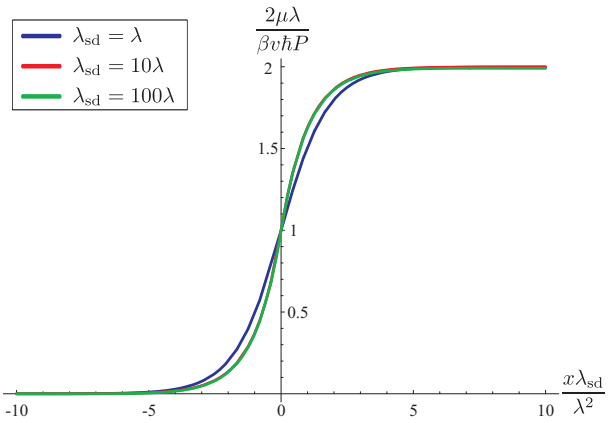

Figure 4.2: Electrochemical potential as a function of position. Note that the potential is proportional to the polarization and that on the horizontal axis the position x is multiplied by the spin-diffusion length.

To find the voltage for all fields B we generalize the results for the voltage difference in Ref. [15] for general domain-wall charge Q. A general expression for the voltage in one dimension is given by [15]

$$\Delta\mu = -\frac{\hbar\mathcal{P}}{2|e|}\int dx\,[\mathbf{\Omega}\cdot(\partial_t\mathbf{\Omega}\times\partial_x\mathbf{\Omega}) + \beta\partial_t\mathbf{\Omega}\cdot\partial_x\mathbf{\Omega}]\ . \tag{4.6}$$

We insert the ansatz [Eq. (4.5) with $\phi(x,t) = \phi(t)$] into Eq. (4.6) and find

$$\Delta\mu = -\frac{\hbar\mathcal{P}}{2|e|}\left[Q\dot{\phi} + \beta\frac{\dot{X}}{\lambda}\right]\ . \tag{4.7}$$

To find a time-averaged value for the voltage we consider the equations of motion for a domain wall that is driven by a transverse magnetic field B [11, 61, 62], contributing to the energy $-g\mathbf{B}\cdot\mathbf{\Omega}$, with $g > 0$. The equations of motion for $X(t)$ and $\phi(t)$ are ultimately derived from the spin-transfer torque equation in Eq. (4.4), and given by

$$\begin{aligned}(1+\alpha^2)\dot{\phi} &= -\frac{gB}{\hbar} - \alpha\frac{K_\perp}{\hbar}\sin(2\phi)\ ,\\ (1+\alpha^2)\frac{\dot{X}}{\lambda} &= \alpha Q\frac{gB}{\hbar} - Q\frac{K_\perp}{\hbar}\sin(2\phi)\ .\end{aligned} \tag{4.8}$$

Here, $K_\perp$ is the out-of-plane anisotropy constant. These equations are solved by

$$\langle \dot{\phi} \rangle = -\frac{\mathrm{Sign}(B)}{1+\alpha^2}\mathrm{Re}\left[\sqrt{\left(\frac{gB}{\hbar}\right)^2 - \left(\frac{\alpha K_\perp}{\hbar}\right)^2}\right],$$
$$\langle \dot{X} \rangle = \frac{\lambda Q}{\alpha}\left(\frac{gB}{\hbar} + \langle \dot{\phi} \rangle\right), \tag{4.9}$$

where $\langle .. \rangle$ denotes a time average. It follows that the voltage difference for general topological charge is

$$\Delta\mu = -\mathrm{Sign}(B)\frac{Q}{1+\alpha^2}\frac{\hbar\mathcal{P}}{2|e|}\left\{(1+\alpha^2)\frac{\beta}{\alpha}\frac{g|B|}{\hbar}\right.$$
$$\left. -\left(1+\frac{\beta}{\alpha}\right)\mathrm{Re}\left[\sqrt{\left(\frac{gB}{\hbar}\right)^2 - \left(\frac{\alpha K_\perp}{\hbar}\right)^2}\right]\right\}. \tag{4.10}$$

Note that the overall prefactor $\mathrm{Sign}(B)Q$ makes sense: inversion of the magnetic field should have the same result as inversion of the topological charge.

In the above, we used a domain-wall ansatz with magnetization perpendicular to the wire direction. Using the topological argument by Yang et al [54]. one can show that the result is more general and holds also for head-to-head and tail-to-tail domain walls. Therefore, for a one-dimensional domain wall, the reactive and dissipative contributions, *i.e.,* the contributions with and without β in the above expression, to the voltage always have opposite sign.

4.4 Vortex domain wall

For more complicated two-dimensional structures the spin-motive force field can have rotation and the simplified expression in Eq. (4.6) is no longer valid so that we need to treat the full potential problem in Eqs. (4.1-4.3). Motivated by recent experimental results [20] we consider in this section the voltage induced by a moving vortex domain wall.

We study the magnetization dynamics using a micro-magnetic simulator [63] from which we obtain the magnetization $\mathbf{\Omega}(\vec{x},t)$. This simulator solves the spin-transfer torque equation in Eq. (4.4). For comparison with the experiment by Yang *et al.* [20], we simulate a permalloy sample that has the same dimensions as this experiment, *i.e.* 20nm $\times$ 500nm $\times$ 32μm, which is divided in 1 $\times$ 128 $\times$ 8192 lattice points. On this sample, we drive a head-to-head vortex domain wall by means of a magnetic field that is pointing from right to left, such that the vortex moves from right to left. For

several field strengths, we obtain the magnetization $\mathbf{\Omega}$, and its time-derivative which allows us to compute the force field $\mathbf{F}$ at each lattice point. Next, we solve the matrix problem that is the discrete equivalent to the potential problem in Eqs. (4.2) and (4.3). For details on this calculation, see Appendix 4.8.

We first investigate the velocity of the vortex domain wall as a function of the applied field. We use the value $\alpha = 0.02$ for the Gilbert-damping parameter to obtain the curve in Fig. 4.3.

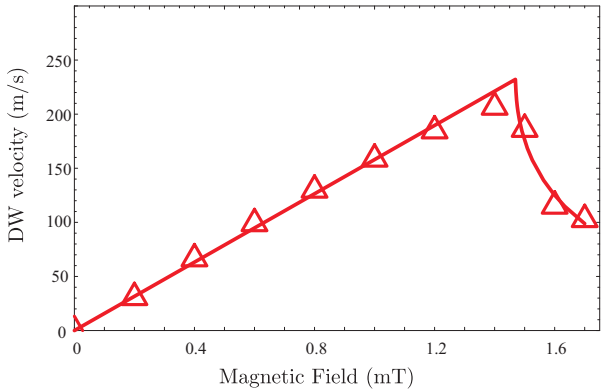

Figure 4.3: Velocity of the vortex domain wall as a function of the magnetic field strength for $\alpha = 0.02$. Above Walker breakdown, the velocity is time-averaged. The line is a guide to the eye.

The decrease in velocity for $B = 1.5$ mT signals Walker breakdown. Indeed, up to fields $B = 1.4$ mT, the vortex moves parallel to the long direction of the sample. For $B = 1.5$ mT, the vortex domain wall motion is more complicated and has a perpendicular component [26, 64]. We therefore expect that below Walker breakdown, just like for the one-dimensional domain wall, the vortex domain wall only has a dissipative contribution to the voltage. Comparison with the experimental results of Ref. [20] shows that our velocity is roughly a factor 2 higher. This might be partly caused by a difference in damping and partly by the presence of defects in the experiment which causes pinning and therefore a decrease of velocity. The exact value of the Walker breakdown field is hard to compare, since this depends also on the exact value of the anisotropy. Nonetheless our value for the Walker breakdown field is of the same order as Ref. [20]. Moreover, what is more important is the dependence of wall velocity and wall-induced voltage on the magnetic field normalized to the Walker-breakdown field, as these results depend less on system details.

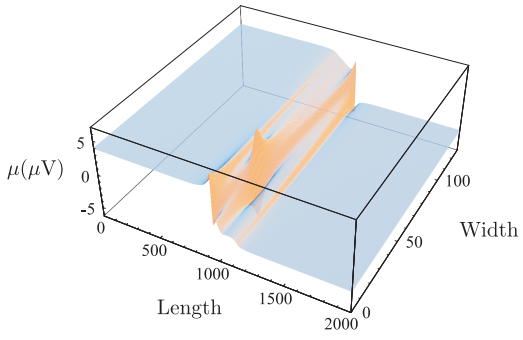

Figure 4.4: Electrochemical potential as a function of position for a moving vortex domain wall on the sample. The numbers on the horizontal axes correspond to lattice points with separation $a = 3.9$nm. This specific figure is for $\alpha = 0.02$, $H = 0.8$mT (*i.e.* below Walker breakdown), $\mathcal{P} = 1$ and $\lambda_{\rm sd} = a$. Note that the peak signals the position of the vortex core.

An example of a specific form of the electrochemical potential on the sample due to a field-driven vortex domain wall is depicted in Fig. 4.4. We see that there is a clear voltage drop along the sample, like in the one-dimensional model. Additionally, the potential shows large gradients around the vortex core and varies along the transverse direction of the sample. For each field strength, we compute the voltage difference as a function of time. For field strengths below Walker breakdown we find that, as expected, only the dissipative term contributes and the voltage difference rapidly approaches a constant value in time. This is understood from the fact that in this regime, the wall velocity is constant after a short time. The dissipative contribution to the voltage is closely related to the velocity along the sample, as can be seen from the red curve in Fig. 4.6.

Above Walker breakdown the reactive term contributes. We find that for $\beta = \alpha$, the oscillations in the reactive component compensate for the oscillations in the dissipative component. If we look closely to Fig. 4.5 we see that the length of the periods is not exactly equal. The periods correspond to a vortex moving to the upper edge of the sample, or to the lower edge. The difference is due to the initial conditions of our simulation. We average the voltage difference over time to arrive at the result in Fig. 4.6. We see that the dissipative contribution becomes smaller for fields larger than the Walker breakdown field, whereas the reactive contribution has the same sign and increases. In fact, for $\beta = \alpha$, the reduction of the dissipative contribution is exactly compensated by the reactive contribution. The β dependence is illustrated in Fig. 4.7. The behavior is fundamentally different from the one-dimensional domain-

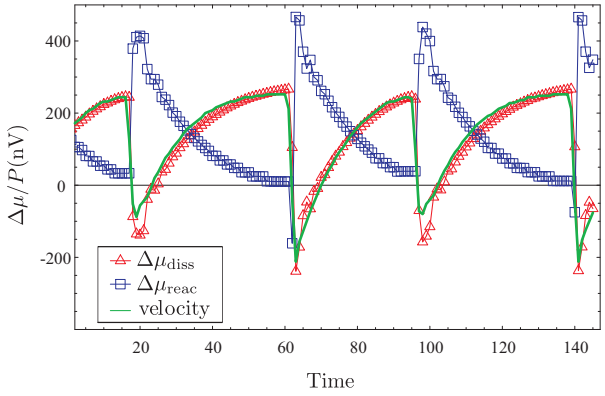

Figure 4.5: Reactive (blue squares) and dissipative (red triangles) contributions to the voltage as a function of time. The numbers on the horizontal axis correspond to time steps of 0.565 ns. The green line gives the velocity along the sample, it is scaled to show the correlation with the voltage. These curves are taken for $\alpha = 0.02$, $\beta = \alpha$ and field strength $B = 1.6$mT.

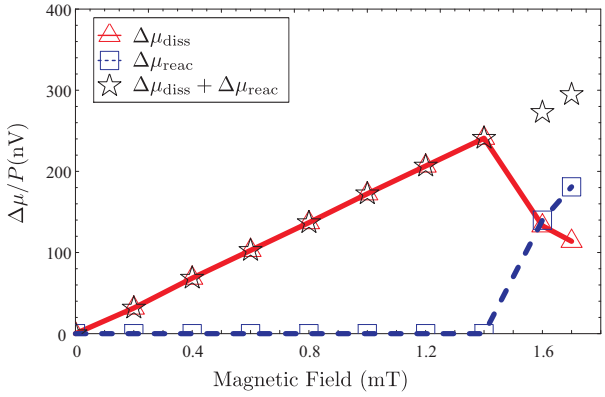

Figure 4.6: Voltage drop along the sample for $\alpha = 0.02$ and $\beta = \alpha$.

wall situation: for the vortex domain wall, the dissipative contribution has the same sign as the reactive contribution.

In order to understand the relative sign, we now discuss general vortex domain walls. A single vortex (*i.e.* with vorticity $q = +1$) is described by two parameters: the charge $p = \pm 1$ indicates wether the central magnetic moment points in the positive or negative z-direction and the chirality C indicates wether the magnetic moments align in a clockwise ($C = -1$) or anti-clockwise ($C = +1$) fashion. We have a vortex that is

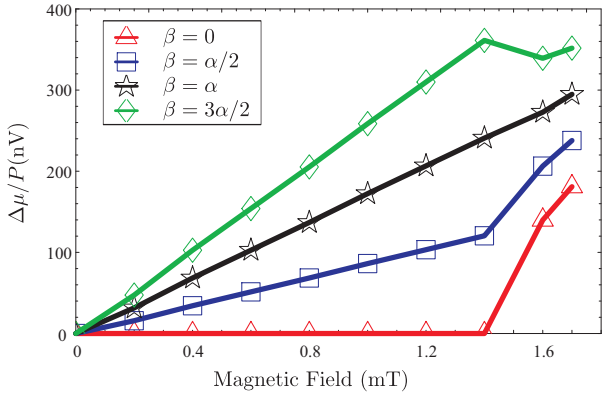

Figure 4.7: Voltage drop along the sample for $\alpha = 0.02$ and several values for β.

oriented clockwise $C = -1$. The relative sign is explained from a naive computation of the voltage above Walker breakdown that does not take into account the rotation of the spin-motive force field

$$\begin{aligned}\Delta\mu &\propto -\int d\vec{x}[\beta\partial_t\mathbf{\Omega}\cdot\partial_x\mathbf{\Omega}+\mathbf{\Omega}\cdot(\partial_t\mathbf{\Omega}\times\partial_x\mathbf{\Omega})]\\ &= \beta v_x\int d\vec{x}(\partial_x\mathbf{\Omega})^2+v_y\int d\vec{x}\mathbf{\Omega}\cdot(\partial_y\mathbf{\Omega}\times\partial_x\mathbf{\Omega})\\ &\propto (\beta\delta+1)v_x\,. \end{aligned} \tag{4.11}$$

where δ is a positive number and we used that above Walker breakdown $\mathbf{\Omega}\simeq\mathbf{\Omega}(x-v_xt, y-v_yt)$ with $v_x\neq 0$ and $v_y\neq 0$. Note that if $v_y = 0$ (below Walker breakdown) the reactive term, *i.e.*, the second term in the above expression, indeed vanishes. We used in the last line that above Walker breakdown $v_x\propto -pv_y$ and $\int d\vec{x}\mathbf{\Omega}\cdot(\partial_y\mathbf{\Omega}\times\partial_x\mathbf{\Omega})\propto -p$. The former equality is understood from a geometric consideration: consider a sample with a vortex characterized by $C = 1$, $p = 1$ and $v_xv_y < 0$. By symmetry, this is equivalent to $C = -1$, $p = -1$ and $v_xv_y > 0$. It is therefore clear that the sign of v_xv_y depends on either the polarization, or the handedness of the vortex. Since we know from the vortex domain wall dynamics that reversal of the polarization reverses the perpendicular velocity [20], we conclude that v_xv_y does not depend on the handedness of the vortex. The latter equality is understood from a similar argument: $\iint dxdy\mathbf{\Omega}\cdot(\partial_y\mathbf{\Omega}\times\partial_x\mathbf{\Omega})$ changes sign under the transformation $\mathbf{\Omega}\to-\mathbf{\Omega}$. During this transformation, both $p\to -p$ and $C\to -C$, and therefore their product cannot account for the total sign reversal. Therefore, the integral depends on the polarization [54] but not on the handedness of the vortex. The positive number δ is obtained from our nu-

merical simulation, which suggests that the magnetic-field dependence of the voltage is

$$\Delta\mu = \beta B \times \text{constant} + (1-\beta/\alpha)|\Delta\mu_{\text{reactive}}| \,. \tag{4.12}$$

Note that the sign of the relative contributions can also be obtained using the topological argument by Yang et al.[54], which gives the same result.

We compare our results in Fig. 4.7 with the experiment by Yang *et al.* [20]. If we assume that the voltage below Walker breakdown lies roughly on the same line as the voltages above Walker breakdown, their results suggest a slope of 10nV/Oe. For $\mathcal{P} \sim 0.8$, our results suggest a slope of (β/α)14nV/Oe. Taking into account our higher velocity, we find that β in the experiment is somewhat larger than α. The decrease in slope of the voltage in Ref. [20] as Walker breakdown is approached from above also suggests $\beta > \alpha$.

In conclusion, the behavior of the voltage around Walker breakdown allows us to determine the ratio β/α. In experiment, the potential difference as a function of the applied magnetic field would show an upturn or downturn around Walker breakdown as in Fig. 4.7, which corresponds to $\beta < \alpha$ and $\beta > \alpha$, respectively.

4.5 Magnetic vortex on a disk

On small disks (of size μm and smaller) of ferromagnetic material the lowest energy configuration is a vortex. It has been shown that one can let the vortex rotate around its equilibrium position by applying an AC magnetic field [55–57, 59, 77]. This motion gives rise via Eq. (4.1) to a spin motive force on the spins, which induces a voltage on the edge of the disk relative to a fixed reference voltage, *e.g.* the disk center. Ohe *et al.* [60] have shown that the reactive contribution to the spin motive force field can be seen as a dipole that is pointing in the radial direction, *i.e.,* the divergence of the force field consists of a positive and a negative peak along the radial direction (note that the divergence of the force field can be seen as an effective charge). Rotation of this dipole gives rise to an oscillating voltage on the edge of the sample. Here, we consider also the dissipative contribution to the voltage.

We consider a vortex on a disk with radius R that moves around its equilibrium position (*i.e.,* the center of the disk) at a distance r_0 from the center of the disk with frequency ω. We use as a boundary condition that the magnetization on the edge of the disk is pointing perpendicular to the radial direction. In equilibrium, the micro-

magnetic energy density of the form $-J\mathbf{\Omega}\cdot\nabla^2\mathbf{\Omega} - K_\perp m_z^2$ is minimized by

$$\begin{aligned} m_x(x,y) &= \frac{-y}{\sqrt{x^2+y^2}}\cos\left[2\arctan\left(e^{-C\sqrt{x^2+y^2}/\kappa}\right)\right] \\ m_y(x,y) &= \frac{x}{\sqrt{x^2+y^2}}\cos\left[2\arctan\left(e^{-C\sqrt{x^2+y^2}/\kappa}\right)\right] \\ m_z(x,y) &= p\ \sin\left[2\arctan\left(e^{\sqrt{x^2+y^2}/\kappa}\right)\right]\ , \end{aligned} \tag{4.13}$$

where the center of the vortex is chosen at $x = y = 0$. Here $\kappa = \sqrt{K_\perp/J}$ is the typical width of the vortex core. For permalloy this length scale is of the order $\sim$ 10nm. The parameters p and C are defined as before, for definiteness we choose $p = 1$, $C = -1$. To describe clockwise circular motion of the vortex around its equilibrium position at fixed radius r_0 we substitute $x \to x - r_0\sin(\omega t)$ and $y \to y - r_0\cos(\omega t)$. Note that we assume that the form of the vortex is not changed by the motion, which is a good approximation for $r_0 \ll R$.

From the magnetization in Eq. (4.13), we compute the force field using Eq. (4.1). The reactive and dissipative contributions to the divergence of the force field are shown in Fig. 4.8. The direction of the dipoles follows directly from Eq. (4.1) if we realize

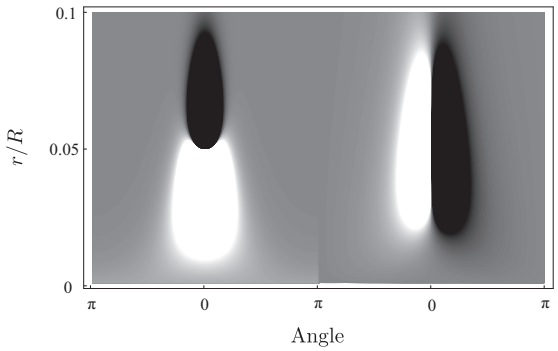

Figure 4.8: The reactive (left) and dissipative (right) contributions to the divergence of the force field. White means positive values, black is negative values. The reactive contribution can be seen as a dipole in the radial direction. The dissipative contribution is a dipole perpendicular to the radial direction.

that for our system $-\partial_t\mathbf{\Omega}\cdot\vec{\nabla}\mathbf{\Omega} = \vec{v}(\partial_{\hat{v}}\mathbf{\Omega})^2$ is always pointing in the direction of the velocity which shows that the dissipative contribution points along the velocity. Likewise the reactive contribution is always pointing perpendicular to the velocity.

From the relative orientations of the effective dipoles, we expect that the peaks in the reactive and dissipative contributions to the voltage on the edge will differ by a

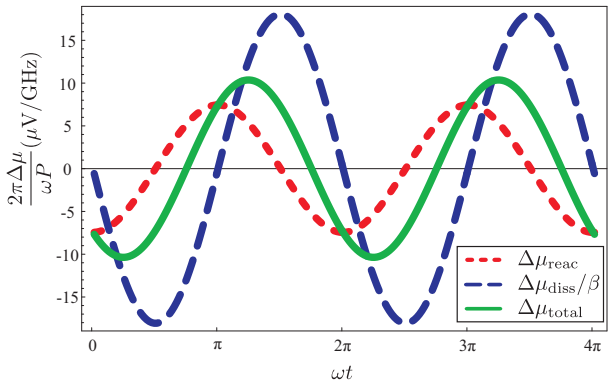

Figure 4.9: The reactive (red dashed curve) and dissipative (blue dashed curve) contributions to the voltage difference between opposite points on the edge of the disk. The green line gives the total voltage difference $\Delta\mu_{\text{total}} = \Delta\mu_{\text{reac}} + \Delta\mu_{\text{diss}}$, in this example for $\beta = 0.4$. We used $r_0 = 10\lambda_{\text{sd}}$, $R = 100\lambda_{\text{sd}}$ and $\kappa = \lambda_{\text{sd}}$. For realistic spin-diffusion length $\lambda_{\text{sd}} \simeq 5$ nm, these parameter values agree with the system of Ohe *et al.*[60].

phase of approximately $\pi/2$ (for $r_0/R \to 0$ this is exact). We divide our sample in 1000 rings and 100 angles and use the general method in Appendix 4.8 to find the voltage on the edge shown in Fig. 4.9.

To compare with Ref. [60], we take a frequency $\omega/(2\pi) = 300$ MHz and $\mathcal{P} = 0.8$, which yields amplitudes for the reactive contribution of $\sim \mu$V on the edge. However, Ohe *et al.* suggest that voltage probes that are being placed closer to the vortex core measure a higher voltage. This indeed increases the voltage up to order $\sim 10\ \mu$V at $r = 2r_0$. Placing the leads much closer to the vortex core does not seem to be realistic because of the size of the vortex. Since the voltage scales with velocity, it can also be increased by a larger radius of rotation, *i.e.* by applying larger magnetic fields. However, for disks larger than 1 μm, the vortex structure is lost.

The dissipative contribution becomes important for large values of β. In principle, it is possible to determine β by looking at the shift of the peak in the total voltage with respect to the peak in the reactive contribution, which is in turn determined by the phase of the applied magnetic field. The phase difference between applied field and measured voltage then behaves as $\tan(\Delta\phi) \propto \beta$.

4.6 Discussion and conclusion

We have investigated the voltage that is induced by a field-driven vortex domain wall in detail. In contrast to a one-dimensional model of a domain wall, the reactive and dissipative contributions to the voltage have the same sign. The qualitative differences for different values of β provide a way to determine the ratio β/α experimentally by measuring the wall-induced voltage as a function of magnetic field. To this end the experimental results in Ref. [20] are in the near future hopefully extended to fields below Walker breakdown, which is challenging as the voltages become smaller with smaller field.

We also studied a magnetic vortex on a disk. When the vortex undergoes a circular motion, a voltage is induced in the sample. Earlier work computed the reactive voltage on the edge of the disk [60], here we include also the dissipative contribution to the voltage. We find that the phase difference between voltage and AC driving field is determined by the β parameter.

4.7 Appendix A: Boundary conditions

As a boundary condition for the potential problems, we demand that the total spin current and charge current perpendicular to the upper and lower boundaries is zero: $j_s^\perp = j_\uparrow^\perp - j_\downarrow^\perp = 0$ and $j^\perp = j_\uparrow^\perp + j_\downarrow^\perp = 0$. Therefore, the majority-and minority spin currents are necessarily zero. They are given by $j_\uparrow = \sigma_\uparrow(F - \nabla\mu_\uparrow)$ and $j_\downarrow = \sigma_\downarrow(-F - \nabla\mu_\downarrow)$. From this, the boundary conditions on the derivatives of the potentials follow as $\partial_\perp\mu_s = \partial_\perp(\mu_\uparrow - \mu_\downarrow)/2 = F$ and $\partial_\perp\mu = \partial_\perp(\mu_\uparrow + \mu_\downarrow)/2 = 0$. We consider a two-dimensional sample that is infinitely long in the x-direction, and of finite size 2Λ in the y-direction. Then, the boundary conditions for the spin accumulation are

$$\partial_y\mu_s(x, y = \pm\Lambda) = F_y(x, y = \pm\Lambda)\,. \tag{4.14}$$

To measure the induced voltage, we also put the derivatives of the potential at infinity to zero so that the boundary conditions for the electrochemical potential are given by

$$\begin{aligned} &\partial_y\mu(x, y = \pm\Lambda) = 0\,, \\ &\partial_x\mu(x \to \pm\infty, y) = 0\,. \end{aligned} \tag{4.15}$$

4.8 Appendix B: Potential problem on a lattice

We consider a two-dimensional lattice, where we have spin accumulation $\mu_s^{i,j}$ and an electrochemical potential $\mu^{i,j}$ at site i, j. Between sites (i, j) and $(i, j+1)$, there can

be a particle current density of majority spins

$$j_{\uparrow,\hat{j}}^{i,j+1/2} = \sigma_\uparrow \left(F_{\hat{j}}^{i,j+1/2} + \frac{\mu_\uparrow^{i,j} - \mu_\uparrow^{i,j+1}}{a_{\hat{j}}^{i,j+1/2}} \right)$$
$$= \sigma_\uparrow \left(F_{\hat{j}}^{i,j+1/2} - \delta_{\hat{j}} \mu_\uparrow^{i,j+1/2} \right) , \tag{4.16}$$

with $a_{\hat{j}}^{i,j+1/2}$ the lattice spacing in the $\hat{j}$-direction between sites (i,j) and $(i,j+1)$, and a particle current density of minority spins

$$j_{\downarrow,\hat{j}}^{i,j+1/2} = \sigma_\downarrow \left(-F_{\hat{j}}^{i,j+1/2} + \frac{\mu_\downarrow^{i,j} - \mu_\downarrow^{i,j+1}}{a_{\hat{j}}^{i,j+1/2}} \right)$$
$$= \sigma_\downarrow \left(-F_{\hat{j}}^{i,j+1/2} - \delta_{\hat{j}} \mu_\uparrow^{i,j+1/2} \right) , \tag{4.17}$$

and equivalently for currents in the $\hat{i}$-direction. The derivative $\delta_{\hat{j}}$ is defined as $\delta_{\hat{j}} O^{i,j} = (O^{i,j+1/2} - O^{i,j-1/2})/a_{\hat{j}}^{i,j}$, and likewise for $\delta_{\hat{i}}$. Note that upper indices (i,j) denote a position on the lattices and lower indices $\hat{i}$ or $\hat{j}$ denote a direction. We can write $\mu_\uparrow = \mu + \mu_\mathrm{s}$ and $\mu_\downarrow = \mu - \mu_\mathrm{s}$. The continuity-like equations for the density of majority- and minority spins are (note that spins move in the direction of the current)

$$A^{i,j} \frac{n_{\uparrow\downarrow}^{i,j}}{\tau} = -\frac{\Delta(\ell^{i,j} j_{\uparrow\downarrow}^{i,j})}{|e|} , \tag{4.18}$$

with characteristic spin-flip time τ and with the dimensionless operator Δ given by

$$\Delta O^{i,j} = O_{\hat{i}}^{i+1/2,j} - O_{\hat{i}}^{i-1/2,j} + O_{\hat{j}}^{i,j+1/2} - O_{\hat{j}}^{i,j-1/2} . \tag{4.19}$$

These definitions allows for non-square lattices with sides at position $(i \pm 1/2, j)$ or $(i, j \pm 1/2)$ that have length $\ell_{\hat{i}}^{i\pm1/2,j}$ or $\ell_{\hat{j}}^{i,j\pm1/2}$ (lower index denotes the normal direction), respectively, and the area of the site itself given by $A^{i,j}$.

The equation for the electrochemical potential is obtained from the continuity equation

$$0 = -|e| A^{i,j} \frac{n_\uparrow^{i,j} + n_\downarrow^{i,j}}{\tau} = \Delta[\ell^{i,j}(j_\uparrow^{i,j} + j_\downarrow^{i,j})] =$$
$$\sigma_\uparrow \Delta[\ell^{i,j}(F^{i,j} - \delta\mu_\uparrow^{i,j})] + \sigma_\downarrow \Delta[\ell^{i,j}(-F^{i,j} - \delta\mu_\downarrow^{i,j})] =$$
$$(\sigma_\uparrow + \sigma_\downarrow)\Delta\{\ell^{i,j}[-\delta\mu^{i,j} + \mathcal{P}(F^{i,j} - \delta\mu_\mathrm{s}^{i,j})]\} .$$

$$\rightarrow \Delta(\ell^{i,j}\delta\mu^{i,j}) = \mathcal{P}\Delta[\ell^{i,j}(F^{i,j} - \delta\mu_\mathrm{s}^{i,j})] , \tag{4.20}$$

where the current polarization is given by $\mathcal{P} = (\sigma_\uparrow - \sigma_\downarrow)/(\sigma_\uparrow + \sigma_\downarrow)$. This result was already obtained for a continuous system in Ref. [14]. To find an equation for the spin accumulation, we write

$$\begin{aligned}
&-|e|A^{i,j}\frac{n_\uparrow^{i,j} - n_\downarrow^{i,j}}{\tau} = \Delta[\ell^{i,j}(j_\uparrow^{i,j} - j_\downarrow^{i,j})] = \\
&\sigma_\uparrow \Delta[\ell^{i,j}(F^{i,j} - \delta\mu_\uparrow^{i,j})] - \sigma_\downarrow \Delta[\ell^{i,j}(-F^{i,j} - \delta\mu_\downarrow^{i,j})] = \\
&(\sigma_\uparrow + \sigma_\downarrow)\Delta\{\ell^{i,j}[F^{i,j} - \delta\mu_{\rm s}^{i,j} - \mathcal{P}\delta\mu^{i,j}]\} = \\
&(\sigma_\uparrow + \sigma_\downarrow)(1-\mathcal{P}^2)\Delta[\ell^{i,j}(F^{i,j} - \delta\mu_{\rm s}^{i,j})] \,. \qquad (4.21)
\end{aligned}$$

If we compare this in the case of a square lattice to the expression in Ref. [14]

$$\frac{1}{\lambda_{\rm sd}^2}\mu_{\rm s} - \nabla^2\mu_{\rm s} = -\boldsymbol{\nabla}\cdot\mathbf{F} \,, \qquad (4.22)$$

we find that the density of spins that pile up can be expressed in terms of the spin accumulation as $(n_\uparrow^{i,j} - n_\downarrow^{i,j})/\tau = (\sigma_\uparrow + \sigma_\downarrow)(1-\mathcal{P}^2)\mu_{\rm s}^{i,j}/(|e|\lambda_{\rm sd}^2)$. We insert this expression to find that the spin accumulation on a lattice is determined by

$$-\frac{1}{\lambda_{\rm sd}^2}\mu_{\rm s}^{i,j} = \frac{1}{A^{i,j}}\Delta[\ell^{i,j}(F^{i,j} - \delta\mu_{\rm s}^{i,j})] \,. \qquad (4.23)$$

Chapter 5

Determination of β from transport coefficients

Abstract

We point out a relation between the dissipative spin-transfer-torque parameter β and the contribution of magnon drag to the thermoelectric power in conducting ferromagnets. Using this result we estimate β in iron at low temperatures, where magnon drag is believed to be the dominant contribution to the thermopower. Our results may be used to determine β from magnon-drag-thermopower experiments, or, conversely, to infer the strength of magnon drag via experiments on spin transfer.

5.1 Introduction

A recurring theme in the field of spintronics is the interplay between electric and spin currents, and magnetization dynamics in conducting ferromagnets. This activity was initiated by the theoretical prediction of Slonczewski [7] and Berger [8] who showed that magnetic layers in nanopillars can be excited or even reversed by spin-polarized currents [65, 66]. As we have seen in Chapter 1, the underlying mechanism is dubbed spin transfer, as it involves the transfer of spin angular momentum from conduction electrons to magnetization. In part because of its promise for applications such as magnetic memories, spin transfer is now actively studied in the context of current-driven domain-wall motion in magnetic nanowires [23, 67–71]. As a result of these efforts, it is now understood [72] that there are at least two contribution to spin transfer in the long-wavelength limit, one reactive (sometimes called adiabatic) [73] and one dissipative [9]. This latter torque is parameterized by a dimensionless constant β, and the ratio of this constant to the Gilbert magnetization damping constant α is of crucial importance for the phenomenology of current-driven domain-wall motion [74, 75].

Precise experimental determination of β from domain-wall experiments [29, 76] or experiments on magnetic vortices [77, 78] is, however, difficult.

A closely-related development is the study of spin and charge currents induced by time-dependent magnetization, called spin pumping in layered systems [48], and usually referred to as spin motive forces in magnetic textures [12]. The latter were observed in a very recent experiment on field-driven domain walls [20], and proposed for magnetic vortices [60]. Like spin transfer, spin motive forces have two contributions corresponding to the reciprocal of the reactive and dissipative spin-transfer torques [14, 15, 79]. In particular, the current induced by a time-dependent magnetization texture also depends on the parameter β.

In this chapter, we show that β is determined by the thermoelectric power due to electron-magnon scattering, the so-called magnon-drag thermopower [80]. This result is derived by considering the electric current density induced by a time-dependent magnetization, as derived in Eq. (1.10). Although this expression is usually considered for magnetization textures such as domain walls or magnetic vortices, it is straightforwardly evaluated for a magnetic configuration corresponding to a transport steady state of (Holstein-Primakoff) magnons. In this chapter, we compute the electric current density that is induced by magnons via spin motive force. This turns out to be linear in β. We relate the result to transport coefficients for the so-called magnon-drag thermopower [80]. In this way, we obtain an expression for β in terms of transport coefficients.

5.2 Spin motive force from magnons

In a ferromagnet, the lowest-energy excitation is a so-called spin wave. A magnon is the quantized version of a spin wave and behaves as a boson. We consider a ferromagnet without anisotropy. First, we compute the dispersion of a magnon in a ferromagnet. We do this by considering a classical plane wave in the magnetization

$$\mathbf{\Omega}(\vec{x},t) = \mathrm{Re}\left[\begin{pmatrix}\delta\Omega_x\\ \delta\Omega_y\\ 1\end{pmatrix} e^{i\vec{k}\cdot\vec{x}-i\omega t}\right] , \tag{5.1}$$

where $\delta\Omega_x$ and $\delta\Omega_y$ are small variations away from the bulk magnetization in the z-direction. From the LLG equation in Eqs. (1.1) and (1.2) (we ignore damping, tem-

perature, and external fields and potentials), we see that

$$\frac{\partial \mathbf{\Omega}}{\partial t} = \frac{J}{\hbar}\mathbf{\Omega} \times \nabla^2 \mathbf{\Omega} \qquad \rightarrow \qquad -i\omega\delta\Omega_x = -\frac{J}{\hbar}k^2\delta\Omega_y \,, \\ -i\omega\delta\Omega_y = \frac{J}{\hbar}k^2\delta\Omega_x \,, \tag{5.2}$$

from which we find a quadratic dispersion relation $\hbar\omega_k = Jk^2$ with $\delta\Omega_y = \pm i\delta\Omega_x$.

The next step is to calculate the spin motive force that is induced by magnons. We start with the spin density operator in the ferromagnet

$$\hat{\boldsymbol{S}}(\vec{x},t) = \begin{pmatrix} \delta\hat{S}_x \\ \delta\hat{S}_y \\ S \end{pmatrix} \,. \tag{5.3}$$

Again, we assume that δS_x and δS_y are small deviations from the z-direction. The excitations can be written in terms of bosonic creation operators $\hat{b}^\dagger$ and annihilation operators $\hat{b}$ using a so-called Holstein-Primakoff transformation

$$\begin{pmatrix} \delta\hat{S}_x \\ \delta\hat{S}_y \\ S \end{pmatrix} = S \begin{pmatrix} \frac{1}{2}(\hat{b}+\hat{b}^\dagger) \\ \frac{1}{2i}(\hat{b}-\hat{b}^\dagger) \\ 1 \end{pmatrix} \,. \tag{5.4}$$

The operators $\hat{b}$ and $\hat{b}^\dagger$ obey the usual bosonic commutation relations. In this way, the spin waves are quantized, *i.e.*, we now have magnons. We insert Eq. (5.4) into the expression for the spin motive force in Eq. (1.10) (we substitute back $\mathbf{\Omega} \rightarrow \hat{\boldsymbol{S}}/S$ and use that the time evolution of the bosonic operators is given by $\hat{b}_{\vec{k}}(t) = e^{\frac{i}{\hbar}\hat{H}t}\hat{b}_{\vec{k}}e^{-\frac{i}{\hbar}\hat{H}t}$ with $\hat{H} = \sum_{\vec{k}}\hbar\omega_{\vec{k}}\hat{b}^\dagger_{\vec{k}}\hat{b}_{\vec{k}}$, *i.e.*, we ignore interactions) and Fourier tranform to find that the expectation value of the current density is given by

$$\langle j\rangle_i = \beta P\frac{\hbar\gamma\sigma}{|e|M_s}\int\frac{d\vec{k}}{(2\pi)^3}\,\hbar\omega_{\vec{k}}k_i g(\vec{k}) \,, \tag{5.5}$$

with a the lattice spacing and $g(\vec{k}) = \langle\hat{b}^\dagger_{\vec{k}}\hat{b}_{\vec{k}}\rangle$ the distribution function of magnons with momentum $\vec{k}$, $\langle..\rangle$ denotes the expectation value. Note that only the dissipative term gives a contribution to the induced current. The magnons that flow through the ferromagnet also represent a heat current density $j_{Q,m}$

$$\langle j_{Q,m}\rangle_i = \int\frac{d\vec{k}}{(2\pi)^3}\,\hbar\omega_{\vec{k}}\frac{\partial\omega_{\vec{k}}}{\partial k_i}g(\vec{k}) \,. \tag{5.6}$$

We combine Eqs. (5.5) and (5.6) to find

$$\vec{j} = \beta\frac{\hbar^2\gamma P\sigma}{2|e|M_s J}\vec{j}_{Q,m} \,, \tag{5.7}$$

where M_s is the saturation magnetization density, and γ is the (minus) gyromagnetic ratio. Equation (5.7) shows that a magnon heat current $\vec{j}_{Q,m}$ results in an electrical current $\vec{j}$. One assumption leading to the above result is that the energy of magnons with wave vector $\vec{k}$ is equal to $\hbar\omega_{\vec{k}} = Dk^2$, in terms of the spin stiffness D. This is a valid approximation for temperatures larger than the magnon gap, which is typically ~ 1 K in metallic ferromagnets. In principle, we cannot exclude a contribution of order α to the right-hand side of Eq. (5.7), coming from the first term in Eq. (1.10). However, if $\alpha \ll \beta$ this correction would be small. (Experimental results on permalloy put β in the range $\geq \alpha$ [29, 77], and $\beta \gg \alpha$ has been reported in some of these experiments.)

5.3 Transport coefficients

To understand how the above result is related to magnon-drag thermopower, we consider the response of the system to electric field $\vec{E}$, magnon-temperature and electron-phonon-temperature gradients, denoted by $\vec{\nabla}T_m$ and $\vec{\nabla}T_{e,p}$, respectively. Introducing two different temperatures for these subsystems is in the present case needed to make connection with the result in Eq. (5.7). We note that in theoretical discussions [81] of the spin-Seebeck effect [82] such temperature differences are also invoked. The linear-response coefficients are determined by

$$\begin{pmatrix} \vec{j} \\ \vec{j}_Q \\ \vec{j}_{Q,m} \end{pmatrix} = \begin{pmatrix} \sigma & \sigma S_{e,p} T & \sigma S_m T \\ \sigma S_{e,p} T & \kappa'_{e,p} T & \zeta T \\ \sigma S_m T & \zeta T & \kappa'_m T \end{pmatrix} \begin{pmatrix} \vec{E} \\ -\frac{\vec{\nabla} T_{e,p}}{T} \\ -\frac{\vec{\nabla} T_m}{T} \end{pmatrix}, \tag{5.8}$$

where $\vec{j}_Q$ is the heat current carried by electrons and phonons. In the above, the magnon-drag thermopower is denoted by S_m, and the magnon heat conductivity at zero electric field by κ'_m. The contribution of electrons and phonons to the thermopower is denoted by the Seebeck coefficient $S_{e,p}$, and their heat conductivity at zero field by $\kappa'_{e,p}$. Drag effects between magnon heat currents and electron-phonon heat currents are denoted by ζ. Also note that we have used Onsager relations to eliminate the Peltier coefficients.

It is important to point out that disentangling heat currents in the above way only applies to weakly-coupled situations. In case this is not possible, such that only the total Seebeck coefficient and thermal conductivity can be measured, our results below are applicable to the case that the thermal transport is dominated by magnons.

The result in Eq. (5.7) applies to the situation that the electron-phonon temperature gradient and electric field are zero. Taking $\vec{E} = \vec{\nabla} T_{e,p} = 0$ and $\vec{\nabla} T_m \neq 0$, we find a magnon heat current and a charge current that are proportional to $\vec{\nabla} T_m$ such that we have $\vec{j} = \vec{j}_{Q,m} \sigma S_m / \kappa_m'$. We combine this with Eq. (5.7) to find our main result

$$\beta = \frac{2|e| M_s D}{\hbar^2 \gamma P} \frac{S_m}{\kappa_m'} \,. \tag{5.9}$$

This result relates the spin-torque parameter β to the magnon-drag thermopower and the magnon heat conductivity at zero field κ_m'. The magnon heat conductivity κ_m at zero electric current, defined by $j_{Q,m} = -\kappa_m \nabla T$ with $T_m = T_{e,p} = T$, in terms of the above transport coefficients, is given by $\kappa_m = \kappa_m' + \zeta - \sigma S_m (S_{e,p} + S_m) T$. The last correction is small in most materials, except for very good thermoelectric materials. Assuming that the magnon-electron heat drag is small, *i.e.*, $\zeta \ll \kappa_m'$, we take $\kappa_m' \approx \kappa_m$ in our estimates. Furthermore, we note that possible corrections of order α to the right-hand side of Eq. (5.7) that we mentioned previously, would lead to similar corrections to the right-hand side of the above result, and are again negligible provided $\beta \gg \alpha$.

5.4 Discussion and conclusion

We now estimate β using available experimental data on magnon-drag thermopower and magnon heat conductivity. In this order-of-magnitude estimate we take, for simplicity, $P = 1$, $\gamma = 2\mu_B/\hbar$ (μ_B is the Bohr magneton) and $M_s = \mu_B / a^3$ with $a \simeq 0.3$ nm a typical lattice constant. According to Blatt *et al.* [83], the main contribution to the thermopower in iron at low temperatures is due to magnon drag and they give the result $S_m \approx 0.016\ (T/K)^{3/2}\ \mu\mathrm{V/K}$. Hsu and Berger [84] find the value of $\kappa_m = 4.9 \times 10^{-2}$ W/K m for $Fe_{95}Si_5$ at 4 K (the iron is silicon doped to decrease the electronic contribution to the heat conductivity). Using a typical value $D = 4 \times 10^{-40}$ J m^2 [84] for the spin stiffness, we find that $\beta \approx 0.1$ at 4 K. The main uncertainty in our estimate is the value of κ_m which is difficult to measure. Nonetheless, this value for β seems not unreasonable as room-temperature values for this parameter obtained from spin-transfer experiments usually find that $\beta \sim 0.1 - 0.01$ for Permalloy [29, 77]. We also point out that the $T^{3/2}$ temperature scaling of S_m would imply, according to Eq. (5.9), that $\kappa_m \propto T^{3/2}/\beta$. It can be shown, on the other hand, that $\kappa_m \propto T^{3/2}/\alpha$ [85] within the Landau-Lifshitz-Gilbert phenomenology, suggesting the ratio β/α is insensitive to temperature, which, in turn, is supported by microscopic calculations [75, 87].

The transport coefficients in Eq. (5.8) determine the dissipation, which must be positive by the second law of thermodynamics. This imposes the condition that the

determinant of the response matrix be positive, which is satisfied if

$$T\sigma\left(\frac{S_{e,p}^2}{\kappa'_{e,p}}+\frac{S_m^2}{\kappa'_m}\right)+\frac{\zeta}{\kappa'_{e,p}\kappa'_m}\left(\zeta-2S_{e,p}S_m\right)\leq 1\ . \tag{5.10}$$

It is conventional to define $Z'_{e,p}=\sigma S_{e,p}^2/\kappa'_{e,p}$, $Z'_m=\sigma S_m^2/\kappa'_m$, so that this relation reads $Z'_{e,p}T+Z'_mT\leq 1$, where we assumed $\zeta\ll\kappa'_m$ like before. Using Eq. (5.9), this condition imposes an upper bound on β:

$$\beta\leq\frac{2|e|M_sD}{\hbar^2\gamma P}\frac{1}{\sigma S_mT}\left(1-Z'_{e,p}T\right)\ , \tag{5.11}$$

where σS_m and γP are assumed positive, which is typically the case. Using the same values as in our previous estimate and taking $Z'_{e,p}T\ll 1$, we find that $\beta\lesssim 1$ at 4 K, using a value of $\sigma\approx 10^{11}\ \Omega\,\mathrm{m}$ at 4 K [86]. This result gives an upper bound for β for a material, which is particularly useful when looking for materials with large β. This is of particular interest for spintronics applications, since large β implies a large current-to-domain-wall coupling, as was shown in Eq. (1.17).

In conclusion, we have shown that the spin-transfer-torque parameter β is related to the ratio of the magnon-drag thermopower and the magnon heat conductivity. From an experimental point-of-view this relation can be used to either determine β experimentally, or to obtain information on the contribution of magnons to heat conduction and thermopower from experimental knowledge of β. From a theoretical point-of-view the relation derived in this letter opens the way for methods to calculate β. The microscopic calculations in the literature usually focus on the contribution to β due to spin-dependent disorder scattering [75, 87–90] or take into account scattering phenomenologically [90]. In future work we intend to microscopically determine β by calculating the magnon-drag thermopower and magnon heat conductivity and then using the relation in Eq. (5.9). With respect to this it is important to mention that the relation in Eq. (5.9) contains all contributions to β provided that $\beta\gg\alpha$. We expect that using this relation will be particularly useful in determining the temperature dependence of β.

The work in this chapter was supported by the Alfred P. Sloan Foundation, and by the NSF under Grant No. DMR-0840965.

Summary

Data in a computer is stored as long strings of ones and zeros. In a magnetic hard disk (which is the most common hard disk), these bits are physically represented by small magnetic domains. A domain with a certain magnetization then means 'one', and a domain with opposite magnetization means 'zero'. The field of research that, among many other subjects, deals with manipulation of small magnetic domains using electric current is called *spintronics*. Here, as an addition to electronics, the spin of the electrons is also used to manipulate the device. Classically, 'spin' is the rotation of an object around its own axis. The spin of an electron can be seen as the quantum-mechanical version of this classical concept. Up to now, one of the great successes of spintronics is so-called giant magneto resistance, a technique used for reading out most modern hard disks.

The subject of this thesis is the dynamics of domain walls. To understand what a domain wall is, we should first look at ferromagnets. The most well-known example of a ferromagnetic material is iron. Magnetic materials consist of atoms that have a small magnetic moment. As long as these magnetic moments point in random directions, the magnetization of the particles cancels, and the overall magnetization of the material is zero (figure a). What is special about a ferromagnet is that here, below a certain temperature, the magnetic moments tend to align in one direction. In this way, magnetic domains with typical sizes of the order of 10 micrometer form with aligned magnetization, so that there is a total magnetization. When you consider a large piece of iron, you will not see much of this magnetization, because there will be a lot of magnetic domains that again cancel each others magnetization (figure b). You can, however, align the domains when you hold a magnet close to the iron, and you will notice that the iron is indeed magnetic afterwards (figure c).

The area where two magnetic domains meet is called a domain wall (figure 1.1 in the introduction). In an experiment, you can force two domains to have opposite magnetization, and thus create a well-defined domain wall. In the domain wall, the magnetization rotates from one domain to the other. The distance over which the magnetization is switched is typically of the order of 10 nanometer. The exact direction

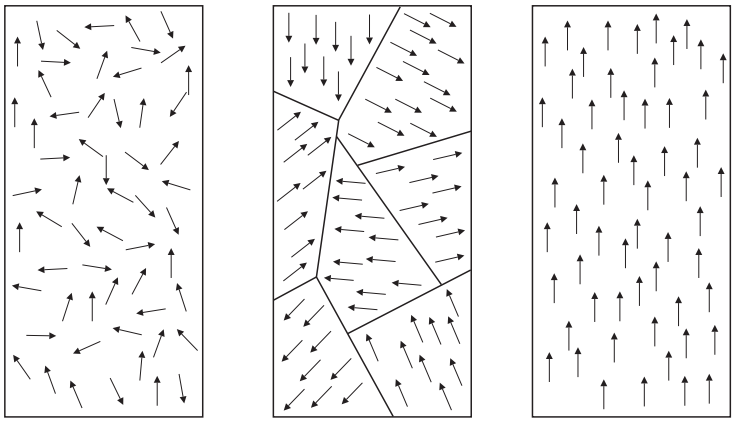

(a) Non-Ferromagnetic material

(b) Ferromagnet with domains

(c) Magnetized ferromagnet

of the magnetic moments in the domain wall is not always straightforward. So-called vortex domain walls turn out to be common in experiments (see figure 1.4 in the introduction). The dynamics of these domain walls is quite diverse. For example, you can move them by applying a magnetic field or by applying an electric current, and you can hold them in place by manipulating the material in several ways.

In this thesis, we study some aspects of domain walls. One of the questions that is addressed is: how does a domain wall react to temperature? In general, temperature makes objects move randomly. This can cause problems if you want a domain wall to stay in place for a long time (you can probably imagine that domain walls that move randomly are not very useful for data storage). Another question is what the relation is between domain-wall motion and waves in the magnetization (called spin waves or magnons). It turns out that this relation provides an alternative way to characterize current-driven domain-wall motion.

Current does not only move a domain wall, the inverse also happens: a moving domain wall can induce a voltage. We study the exact induced voltage generated by a moving vortex domain wall. This is interesting since the mechanism has been observed in experiment very recently.

Samenvatting

Data in een computer wordt opgeslagen als een lange keten van enen en nullen. In een magnetische harde schijf (de meest gebruikte harde schijf) zijn deze bits kleine magnetische gebiedjes (domeinen). Een domein met een bepaalde magnetisatie betekent dan een één, terwijl een domein met tegenovergestelde magnetisatie een nul is. Het onderzoeksgebied dat, naast andere onderwerpen, kijkt naar de manipulatie van kleine magneetgebieden met behulp van elektrische stroom heet *spintronica*. Als aanvulling op elektronica wordt hierbij ook de spin van de elektronen gebruikt om een apparaat te beinvloeden. Klassiek betekent 'spin' dat een voorwerp ronddraait om zijn eigen as. De spin van een elektron kan worden gezien als de kwantummechanische variant van dit klassieke begrip. Een van de grootste successen van dit vakgebied is de zogenaamde *giant magneto resistance* (gigantische magnetische weerstand), een techniek die in de meeste moderne harde schijven wordt gebruikt voor het uitlezen van de data.

Het onderwerp van dit proefschrift is de dynamica van domeinwanden. Om te begrijpen wat een domeinwand is moeten we eerst kijken naar ferromagneten. Het meest bekende voorbeeld van een ferromagnetisch materiaal is ijzer. Magnetische materialen bestaan uit atomen die een klein magnetisch moment hebben. Zo lang deze magnetische momenten in willekeurige richtingen wijzen middelen ze elkaar uit, en zal de totale magnetisatie van het materiaal nul zijn (figuur a). De speciale eigenschap van een ferromagneet is dat de magnetische momenten onder een bepaalde temperatuur de neiging hebben dezelfde kant op te wijzen. Hierdoor ontstaan er domeinen met een typische doorsnee van 10 micrometer waar de magnetische momenten dezelfde kant op wijzen, zodat er een totale magnetisatie is. Als je naar een groot stuk ijzer kijkt dan zie je niet veel van deze magnetisatie. Dit komt omdat er heel veel domeinen zijn met ieder een andere magnetisatierichting, waardoor de magnetisatie weer uitmiddelt (figuur b). Je kan de magnetizatie van de domeinen echter dezelfde kant op laten wijzen door een magneet in de buurt van het ijzer te houden. De domeinen zullen zich dan richten naar het magneetveld van de magneet, en je merkt achteraf dat het stuk ijzer inderdaad magnetisch is geworden (figuur c).

Het gebied waar twee domeinen tegen elkaar aankomen wordt een domeinwand

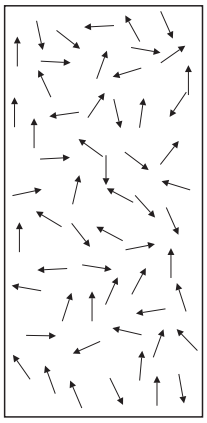

(a) Niet-Ferromagnetisch materiaal

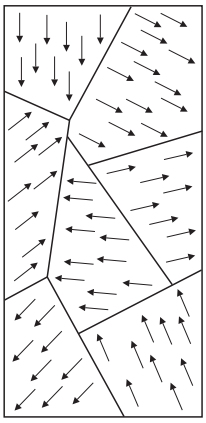

(b) Ferromagneet met domeinen

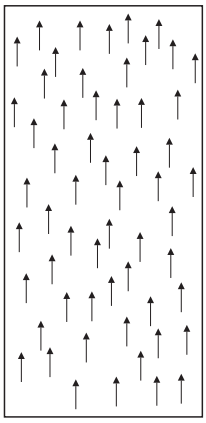

(c) Gemagnetiseerde ferromagneet

genoemd (figuur 1.1 in de introductie). In een experiment kan je er voor zorgen dat je twee domeinen hebt die tegenovergestelde magnetisatie hebben, met daartussen een goed gedefinieerde domeinwand. In de domeinwand draait de magnetizatie van het ene domein naar het andere. De typische afstand waarover dit gebeurt is zo'n 10 nanometer. De precieze richting van de magnetisatie in de domeinwand is niet zo eenvoudig te voorspellen. Zo komen zogenaamde vortex domeinwanden veel voor in experimenten (zie figuur 1.4 in de introductie). De dynamica van domeinwanden is erg divers. Je kan ze bijvoorbeeld in beweging zetten met een magneetveld, maar ook met een elektrische stroom. Ook zijn er verschillende methodes om een domeinwand op een bepaalde plek vast te houden door het materiaal op verschillende manieren te bewerken.

In dit proefschrift bestuderen we enkele aspecten van domeinwanden. Een van de vragen die we ons stellen is: hoe reageert een domeinwand op temperatuur? Over het algemeen zorgt temperatuur ervoor dat objecten willekeurige bewegingen gaan maken. Dit kan een probleem zijn als je wilt dat een domeinwand gedurende langere tijd op dezelfde plek blijft (je kan je wellicht voorstellen dat een willekeurig bewegende domeinwand niet zo nuttig is voor data opslag). Een andere vraag is wat precies de relatie is tussen een bewegende domeinwand en golven in de magnetisatie (deze golven worden spingolven of magnonen genoemd). Het blijkt dat deze relatie een alternatieve methode biedt om stroom-aangedreven domeinwanddynamica te bestuderen.

Stroom kan niet alleen een domeinwand bewegen, het omgekeerde gebeurt ook:

een bewegende domeinwand kan een voltage veroorzaken. We bestuderen in detail het voltage dat een bewegende vortex domeinwand induceert. Dit is interessant omdat dit mechanisme recent is gezien in een experiment. We zijn benieuwd of verdere experimenten die nu worden gedaan aansluiten bij onze voorspellingen.

Dankwoord

In tegenstelling tot sommigen vond ik mijn tijd als promovendus een redelijk ontspannen tijd, zonder noemenswaardige tegenslagen. Daarom lijkt het me wat misplaatst de halve wereld te bedanken voor de steun. In dit dankwoord beperk ik me dan ook tot mensen die direct hebben geholpen met de inhoud van dit proefschrift.

Allereerst is dat mijn begeleider Rembert die met concrete projecten kwam die binnen een jaar te doen zijn. Dat kan niet van elke begeleider gezegd worden. Ik heb je enthousiasme en praktische instelling erg gewaardeerd, zeker ook toen al duidelijk was dat ik niet verder zou gaan in de wetenschap.

In het verlengde hiervan zijn de "BEC meetings" nuttige bijeenkomsten waar domme vragen (die bestaan) gewoon gesteld kunnen worden. Collega promovendi waarmee ik de meeste gesprekken heb gevoerd zijn Erik, Jildou, Shaoyu (postdoc) en niet te vergeten Eelco. Vaak is de vraag stellen hem beantwoorden, maar dat maakt het niet minder nuttig.

De staf van het ITF mag hier niet ontbreken, en dan voornamelijk die op de derde verdieping. Het is goed om te zien dat de hoge heren en dames graag tijd maken voor vragen, ook van andermans promovendi. Christiane tijdens mijn masteronderzoek, Gerard voor programmeerproblemen, René voor Poisson vergelijkingen, Henk voor van alles en nog wat en Paul voor de schaterlach en complottheorieen. Daarnaast heb ik een prettige onderwijssamenwerking gehad met de eerste drie.

Dan is er nog de samenwerking geweest met de groep "Physics of Nanostructures" in Eindhoven welke heeft geleid tot één van de in dit proefschrift opgenomen publicaties. Vooral Geerit wil ik hartelijk bedanken voor het opknappen van het vuile computerwerk. Also I would like to thank Clement Wong and Yaroslav Tserkovnyak for the pleasant collaboration on the last paper.

Misschien niet direct betrokken met de inhoud van het proefschrift, maar toch: Geertje, Els, Olga, Joost, heel erg bedankt.

Dat was het wel zo'n beetje. Nou vooruit, Minne, bedankt voor een stuk of drieduizend lunches de afgelopen twaalf jaar.

Bibliography

[1] A. Aharoni, *Introduction to the Theory of Ferromagnetism*, Clarendon Press (1996).

[2] M. N. Baibich, J. M. Broto, A. Fert, F. Nguyen Van Dau, and F. Petroff, Phys. Rev. Lett. **61**, 2472 (1988).

[3] G. Binasch, P. Grünberg, F. Saurenbach, and W. Zinn, Phys. Rev. B **39**, 4828 (1989).

[4] S.S.P. Parkin, M. Hayashi, and L. Thomas, Science **320**, 190-194 (2008).

[5] L. Berger, J. Appl. Phys. **55**, 1954 (1984).

[6] P.P. Freitas and L. Berger, J. Appl. Phys. **57**, 1266 (1985).

[7] J.C. Slonczewski, J. Magn. Magn. Mater. **159**, L1 (1996).

[8] L. Berger, Phys. Rev. B **54**, 9353 (1996).

[9] S. Zhang and Z. Li, Phys. Rev. Lett. **93**, 127204 (2004).

[10] S.E. Barnes and S. Maekawa, Phys. Rev. Lett. **95**, 107204 (2005).

[11] G. Tatara and H. Kohno, Phys. Rev. Lett. **92**, 086601 (2004); **96**, 189702 (2006).

[12] S.E. Barnes and S. Maekawa, Phys. Rev. Lett. **98**, 246601 (2007).

[13] W.M. Saslow, Phys. Rev. B **76**, 184434 (2007).

[14] Y. Tserkovnyak and M. Mecklenburg, Phys. Rev. B **77**, 134407 (2008).

[15] R.A. Duine, Phys. Rev. B **77**, 014409 (2008).

[16] R.A.Duine, Phys. Rev. B **79**, 014407 (2009).

[17] R.A. Duine, A.S. Núñez, and A.H. MacDonald, Phys. Rev. Lett. **98**, 056605 (2007).

[18] M.E. Lucassen, H.J. van Driel, C. Morais Smith, and R.A. Duine, Phys. Rev. B **79**, 224411 (2009).

[19] J.H. Franken, P. Möhrke, M. Kläui, J. Rhensius, L.J. Heyderman, J.-U. Thiele, H.J.M. Swagten, U.J. Gibson, and U. Rüdiger. Appl. Phys. Lett. **95**, 212502 (2009).

[20] S.A. Yang, G.S.D. Beach, C. Knutson, D. Xiao, Q. Niu, M. Tsoi, and J.L. Erskine, Phys. Rev. Lett. **102**, 067201 (2009).

[21] A. Einstein, Ann. d. Phys. **17**, 549 (1905).

[22] M.J.M. de Jong and C.W.J. Beenakker, in *Mesoscopic Electron Transport*, edited by L.L. Sohn, L.P. Kouwenhoven and G. Schoen, NATO ASI Series (Kluwer Academic, Dordrecht, 1997), Vol. 345, pp. 225-258.

[23] J. Grollier, P. Boulenc, V. Cros, A. Hamzić, A. Vaurès, and A. Fert, Appl. Phys. Lett. **83**, 509 (2003).

[24] M. Kläui, C.A.F. Vaz, J.A.C. Bland, W. Wernsdorfer, G. Faini, and E. Cambril, Appl. Phys. Lett. **83**, 105 (2003).

[25] A. Yamaguchi, T. Ono, S. Nasu, K. Miyake, K. Mibu, and T. Shinjo, Phys. Rev. Lett. **92**, 077205 (2004).

[26] G.S.D. Beach, C. Nistor, C. Knutson, M. Tsoi, and J.L. Erskine, Nature Mat. **4**, 741-744 (2005).

[27] M. Yamanouchi, D. Chiba, F. Matsakura, T. Dietl, and H. Ohno, Phys. Rev. Lett. **96**, 096601 (2006).

[28] M. Hayashi, L. Thomas, C. Rettner, R. Moriya, Y. B. Bazaliy, and S.S.P. Parkin, Phys. Rev. Lett. **98**, 037204 (2007).

[29] L. Heyne, M. Klaüi, D. Backes, T.A. Moore, S. Krzyk, U. Rüdiger, L.J. Heyderman, A. Fraile Rodríguez, F. Nolting, T.O. Mentes, M. Á. Niño, A. Locatelli, K. Kirsch, and R. Mattheis, Phys. Rev. Lett. **100**, 066603 (2008).

[30] M. Feigenson, J.W. Reiner, and L. Klein, Phys. Rev. Lett. **98**, 247204 (2007).

[31] P. Bruno, Phys. Rev. Lett. **83**, 2425 (1999).

[32] J.J. Versluijs, M.A. Bari, and J.M.D. Coey, Phys. Rev. Lett. **87**, 026601 (2001).

[33] N. García, M. Muñoz, and Y.-W. Zhao, Phys. Rev. Lett. **82**, 2923 (1999).

[34] J. Foros, A. Brataas, Y. Tserkovnyak, and G.E.W. Bauer, Phys. Rev. Lett. **95**, 016601 (2005).

[35] A.S. Núñez and R.A. Duine, Phys. Rev. B **77**, 054401 (2008).

[36] A.L. Chudnovskiy, J. Swiebodzinski, and A. Kamenev, Phys. Rev. Lett. **101**, 066601 (2008).

[37] J. Foros, A. Brataas, Y. Tserkovnyak, and G.E.W. Bauer, Phys. Rev. B. **78**, 140402(R) (2008).

[38] H.T.C. Stoof, J. Low Temp. Phys. **114**, 11 (1999).

[39] A. Mitra and A.J. Millis, Phys. Rev. B **72**, 121102(R) (2005).

[40] I.I. Mazin, Phys. Rev. Lett. **83**, 1427 (1999).

[41] X. Waintal and M. Viret, Europhys. Lett. **65**, 427 (2004).

[42] H. Katsura, A.V. Balatsky, Z. Nussinov, and N. Nagaosa, Phys. Rev. B **73**, 212501 (2006).

[43] G. Tatara, Y.-W. Zhao, M. Muñoz, and N. García, Phys. Rev. Lett. **83**, 2030 (1999).

[44] J.M.D. Coey, L. Berger, and Y. Labaye, Phys. Rev. B **64**, 020407(R) (2001).

[45] J.B. Johnson, Nature **119**, 50 (1927); Phys. Rev. **29**, 367 (1927); Phys. Rev. **32**, 97 (1928).

[46] H. Nyquist, Phys. Rev. **29**, 614 (1927); Phys. Rev. **32**, 110 (1928).

[47] J. Xiao, G.E.W. Bauer, S. Maekawa, and A. Brataas, Phys. Rev. B **79**, 174415 (2009).

[48] Y. Tserkovnyak, A. Brataas, and G.E.W. Bauer, Phys. Rev. Lett. **88**, 117601 (2002).

[49] V. Lecomte, S.E. Barnes, J.-P. Eckmann, and T. Giamarchi, Phys. Rev. B **80**, 054413 (2009).

[50] K.M.D. Hals, A.K. Nguyen, and A. Brataas, Phys. Rev. Lett. **102**, 256601 (2009).

[51] L. Berger, Phys. Rev. B **33**, 1572 (1986).

[52] G.E. Volovik, J. Phys. C **20**, L83-L87 (1987).

[53] A. Stern, Phys. Rev. Lett. **68**, 1022 (1992).

[54] S.A. Yang, G.S.D. Beach, C. Knutson, D. Xiao, Z. Zhang, M. Tsoi, Q. Niu, A.H. MacDonald, and J.L. Erskine, Phys. Rev. B **82**, 054410 (2010).

[55] S.-B. Choe, Y. Acremann, A. Scholl, A. Bauer, A. Doran, J. Stöhr, and A.H. Padmore, Science **304**, 420 (2004).

[56] B. Van Waeyenberge, A. Puzic, H. Stoll, K.W. Chou, T. Tyliszczak, R. Hertel, M. Fähnle, H. Brückl, K. Rott, G. Reiss, I. Neudecker, D. Weiss, C.H. Back, and G. Schütz, Nature (London) **444**, 461 (2006).

[57] K.-S. Lee and S.-K. Kim, Appl. Phys. Lett. **91**, 132511 (2007).

[58] M. Bolte, G. Meier, B. Krüger, A. Drews, R. Eiselt, L. Bocklage, S. Bohlens, T. Tyliszczak, A. Vansteenkiste, B. Van Waeyenberge, K.W. Chou, A. Puzic, and H. Stoll, Phys. Rev. Lett. **100**, 176601 (2008).

[59] B. Krüger, A. Drews, M. Bolte, U. Merkt, D. Pfannkuche, G. Meier, Phys. Rev. B **76**, 224426 (2007).

[60] J.-I. Ohe, S.E. Barnes, H.-W. Lee, and S. Maekawa, Appl. Phys. Lett. **95**, 123110 (2009).

[61] N.L. Schryer and L.R. Walker, J. Appl. Phys. **45**, 5406 (1974).

[62] G. Tatara, H. Kohno, and J. Shibata, Physics Reports **468**, 213 (2008).

[63] M.R. Scheinfein, LLG Micromagnetics Simulator, http:// llgmicro.home.mindspring.com.

[64] D.J. Clarke, O.A. Tretiakov, G.-W. Chern, Ya. B. Bazaliy, and O. Tchernyshyov, Phys. Rev. B **78**, 134412 (2008).

[65] M. Tsoi, A.G.M. Jansen, J. Bass, W.-C. Chiang, M. Seck, V. Tsoi, and P. Wyder, Phys. Rev. Lett. **80**, 4281 (1998).

[66] E.B. Myers, D.C. Ralph, J.A. Katine, R.N. Louie, and R. A. Buhrman, Science **285**, 867 (1999).

[67] M. Tsoi, R.E. Fontana, and S.S.P. Parkin, Appl. Phys. Lett. **83**, 2617 (2003).

[68] M. Kläui, C.A.F. Vaz, J.A.C. Bland, W. Wernsdorfer, G. Faini, E. Cambril, L.J. Heyderman, F. Nolting, and U. Rüdiger, Phys. Rev. Lett. **94**, 106601 (2005).

[69] G.S.D. Beach, C. Knutson, C. Nistor, M. Tsoi, and J.L. Erskine, Phys. Rev. Lett. **97**, 057203 (2006).

[70] M. Hayashi, L. Thomas, C. Rettner, R. Moriya and S.S.P. Parkin, Nature Physics **3**, 21 (2007).

[71] M. Yamanouchi, D. Chiba, F. Matsukura, and H. Ohno, Nature **428**, 539 (2004);

[72] G. Tatara, H. Kohno, and J. Shibata, Phys. Rep. **468**, 213 (2008), and references therein.

[73] Ya. Bazaliy, B.A. Jones, and S.-C. Zhang, Phys. Rev. B **57**, R3213 (1998).

[74] A. Thiaville, Y. Nakatani, J. Miltat, and Y. Suzuki, Europhys. Lett. **69**, 990 (2005).

[75] Y. Tserkovnyak, H.J. Skadsem, A. Brataas, and G.E.W. Brataas, Phys. Rev. B **74**, 144405 (2006).

[76] L. Thomas, M. Hayashi, X. Jiang, R. Moriya, C. Rettner, and S.S.P. Parkin, Nature **443**, 197 (2006).

[77] M. Bolte, G. Meier, B. Krüger, A. Drews, R. Eiselt, L. Bocklage, S. Bohlens, T. Tyliszczak, A. Vansteenkiste, B. Van Waeyenberge, K.W. Chou, A. Puzic, and H. Stoll, Phys. Rev. Lett. **100**, 176601 (2008).

[78] L. Heyne, J. Rhensius, D. Ilgaz, A. Bisig, U. Rüdiger, M. Kläui, L. Joly, F. Nolting, L.J. Heyderman, J.U. Thiele, and F. Kronast, Phys. Rev. Lett. **105**, 187203 (2010).

[79] C.H. Wong and Y. Tserkovnyak, Phys. Rev. B **80**, 184411 (2009).

[80] M. Bailyn, Phys. Rev. **126**, 2040 (1962).

[81] J. Xiao, G.E.W. Bauer, K. Uchida, E. Saitoh, and S. Maekawa, Phys. Rev. B **81**, 214418 (2010).

[82] K. Uchida, S. Takahashi, K. Harii, J. Ieda, W. Koshibae, K. Ando, S. Maekawa, and E. Saitoh, Nature (London) **455**, 778 (2008).

[83] F.J. Blatt, D.J. Flood, V. Rowe, P.A. Schroeder, and J.E. Cox, Phys. Rev. Lett. **18**, 395 (1967).

[84] Y. Hsu and L. Berger, Phys. Rev. B **18**, 4856 (1978).

[85] A.A. Kovalev and Y. Tserkovnyak, Europhys. Lett. **97**, 67002 (2012).

[86] W.R.G. Kemp, P.G. Klemens, and G.K. White, Austr. J. Phys **9**, 180 (1956).

[87] H. Kohno, G. Tatara, and J. Shibata, J. Phys. Soc. Japan **75**, 113706 (2006).

[88] F. Piéchon and A. Thiaville, Phys. Rev. B **75**, 174414 (2007).

[89] R.A. Duine, A.S. Núñez, Jairo Sinova, and A.H. MacDonald, Phys. Rev. B **75**, 214420 (2007).

[90] I. Garate, K. Gilmore, M.D. Stiles, and A.H. MacDonald, Phys. Rev. B **79**, 104416 (2009).